Soil Dynamics and Earthquake Engineering 128 (2020) 105874

Contents lists available at ScienceDirect

Soil Dynamics and Earthquake Engineering

journal homepage: http://www.elsevier.com/locate/soildyn

Lateral spreading of ports in the 2014 Cephalonia, Greece, earthquakes

G.A. Athanasopoulos [a,*], G.C. Kechagias [a], D. Zekkos [b], A. Batilas [c], X. Karatzia [d], F. Lyrantzaki [a], A. Platis [e]

[a] Department of Civil Engineering, University of Patras, Greece
[b] Dept of Civil and Environmental Engineering, University of Michigan, 48103, USA
[c] Atkins, The Axis, 10 Holiday Street, Birmingham, UK
[d] HOCHTIEF GmbH Consult IKS, Frankfurt, Germany
[e] Geoconsult Ltd, Athens, Greece

ARTICLE INFO

Keywords:
Lateral spreading
Soil liquefaction
Quay wall
Cephalonia 2014 earthquakes
Ports
Geotechnical data

ABSTRACT

A case history is presented of lateral spreading in two reclaimed port areas of the Cephalonia island, Greece, in the 2014 earthquake doublet (M_w 6.1 & 6). Lateral ground displacements along 24 transects perpendicular to the quay walls in the two port areas were directly measured by ground surveys. Liquefaction of gravel-size fills was observed throughout the ports and was more pronounced in Lixouri port where ground motions were higher. The maximum cumulative horizontal ground displacements ranged from 3 cm to 152 cm, depending on the transect location and height of free face, whereas the inland extent of lateral ground movement ranged from 10 m to 90 m. Lateral movement of the quay walls in Argostoli Port was lower compared to Lixouri Port. Strong motion recordings in the two port areas as well as pertinent seismotectonic data are also presented along with the available geotechnical data compiled by integrating information from exploratory borings, trial pits, site geology and eye-witness accounts of the reclamation history of the areas. Average cumulative lateral displacements for groups of transects, characterized by similar height of quay wall and field conditions were derived and compared to lateral spreading predictions using an empirical relationship for free field conditions. It was found that the magnitude of lateral spreading behind the gravity-type quay walls was significantly lower compared to empirical predictions based on the assumption of free field conditions. The reduction of lateral ground movement depends on the height of quay wall and may even be an order of magnitude lower for wall heights of 6 m or greater. The findings of this study contribute in assessing quay wall movement in port areas especially when liquefaction has occurred behind the wall.

1. Introduction

In early 2014 the island of Cephalonia in Greece, shown in Fig. 1, was shaken by a sequence of two earthquakes: the first event occurred on 26 January 2014 with a magnitude M_w 6.1 whereas the second event took place 8 days later, on 3 February 2014, with a magnitude M_w 6.0. The earthquake doublet - whose epicenters are shown in Fig. 1 - was felt predominantly in Cephalonia, but also throughout the Ionian Islands, as well as in the Peloponnese and the western continental Greece. The response of structures in the area was, in general, satisfactory [56,57]. Most importantly, no human loss of life occurred due to earthquake shaking, despite the high ground accelerations recorded (up to 0.77 g).

The occurrence of the 2014 Cephalonia earthquake doublet resulted in ground failures involving soil liquefaction at the port areas of Lixouri and Argostoli, seaward movements of the multi-block quay walls in these ports, and failures of earth slopes and earth retaining structures, buildings, monuments, and lifeline networks in the Paliki peninsula of western Cephalonia [35]. A consensus exists that the majority of observed damage was caused by the second earthquake event. Issues related to the type and location of the causative faults of the two events and the recorded strong motion characteristics (including manifestation of forward directivity of the fault rupture) were subsequently investigated by several researchers [32–34,51,59,70,74,79].

This paper focuses on the occurrence of damage in the port areas of Lixouri and Argostoli that is caused by a combination of liquefaction-induced lateral spreading and lateral movement and rotation of the

* Corresponding author.
E-mail addresses: gaa@upatras.gr (G.A. Athanasopoulos), gkech89@gmail.com (G.C. Kechagias), zekkos@geoengineer.org (D. Zekkos), an_batilas@hotmail.com (A. Batilas), polyxeni.karatzia@hochtief.de (X. Karatzia), lyrafo@hotmail.com (F. Lyrantzaki), geoconsult@geoconsult.gr (A. Platis).

https://doi.org/10.1016/j.soildyn.2019.105874
Received 31 May 2019; Received in revised form 9 August 2019; Accepted 22 September 2019

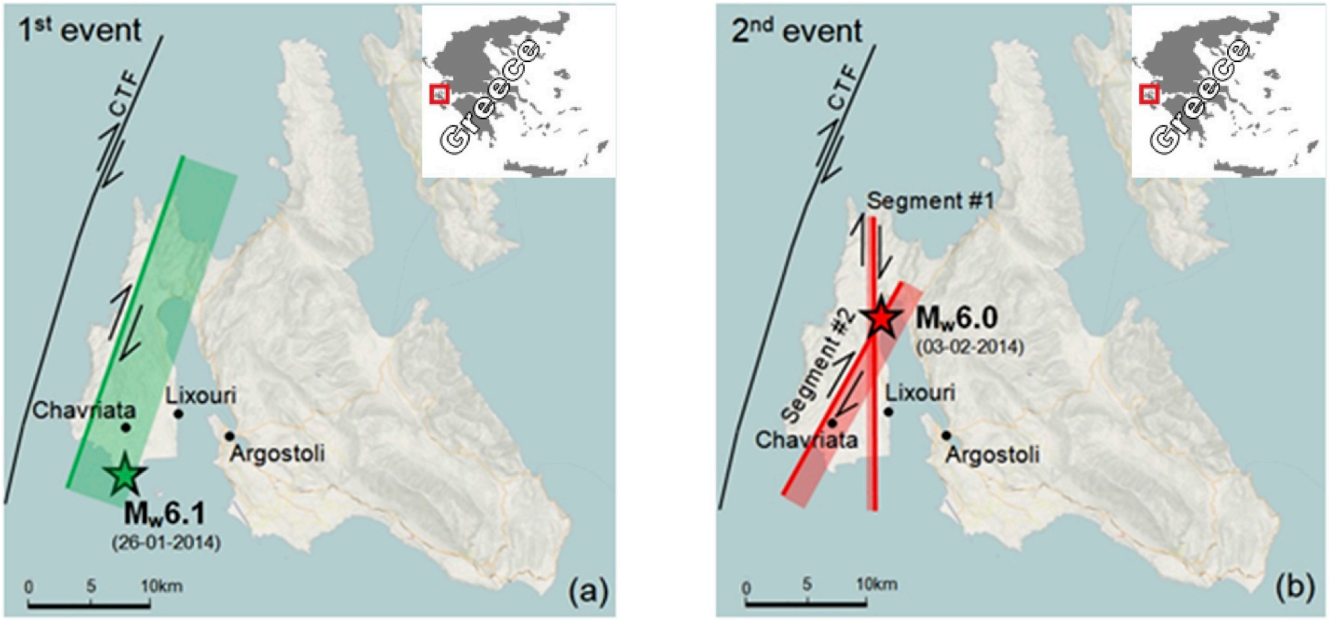

Fig. 1. Epicenters and causative faults of the Cephalonia 2014 earthquake doublet. (a) 1st event, (b) 2nd event (based on [74]).

Fig. 2. Satellite image of the Lixouri Port area (liquefied area indicated by yellow shading and location of photos indicated by numbered white squares). (For interpretation of the references to color in this figure legend, the reader is referred to the Web version of this article.)

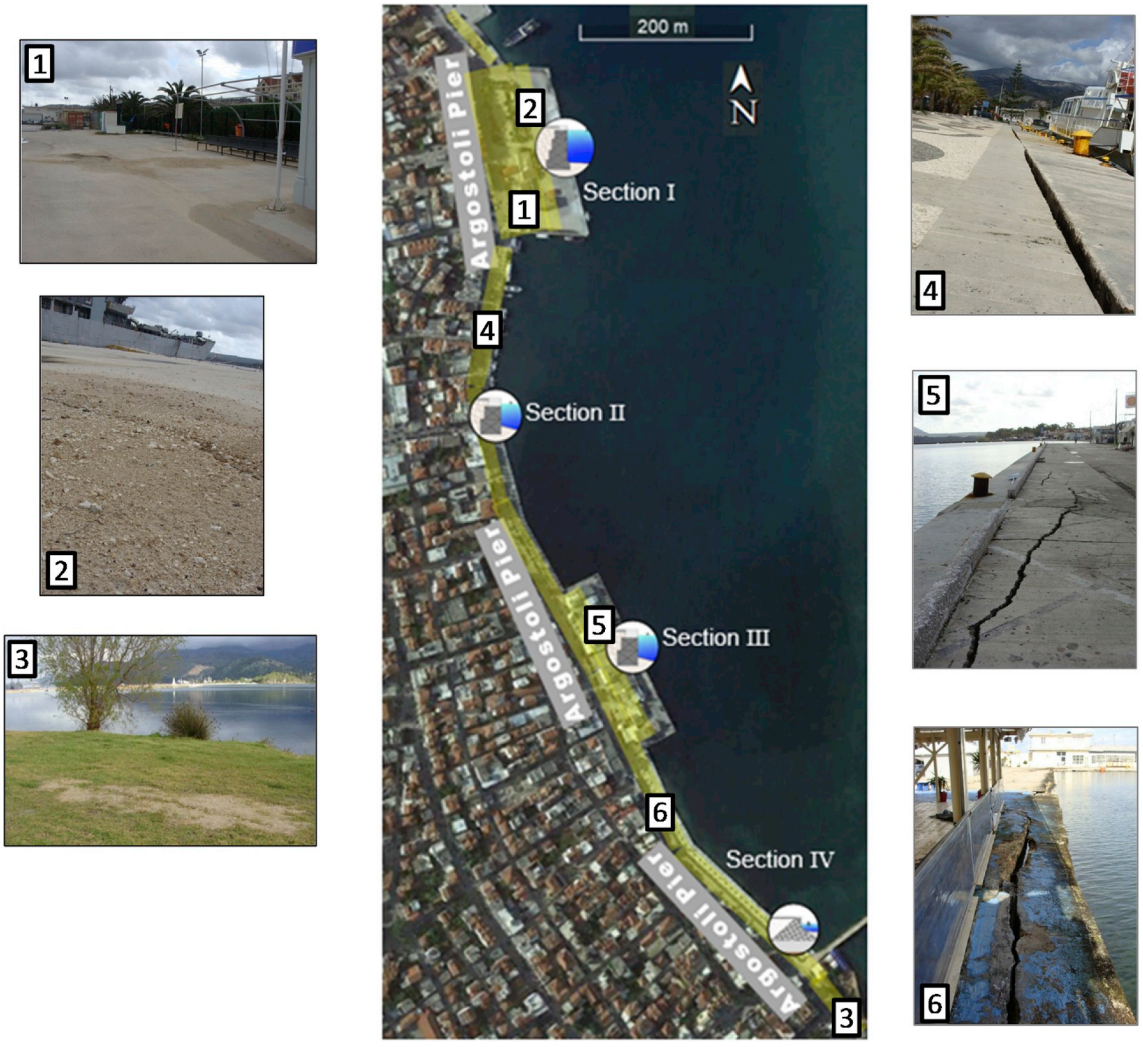

Fig. 3. Satellite image of the Argostoli Port area (liquefied area indicated by yellow shading and location of photos indicated by numbered white squares). (For interpretation of the references to color in this figure legend, the reader is referred to the Web version of this article.)

quay walls. A brief overview of the seismic behavior of soil formations in the two port areas and the performance of quay walls is first presented, followed by the recorded strong motion data and information pertaining to geological, geotechnical and seismotectonic issues. The results of measurements of lateral ground spreading in the Ports of Lixouri and Argostoli following the 2014 earthquakes are then presented along with a review of pertinent literature. Finally, the effect of the multi-block quay walls in reducing the magnitude of lateral spreading of the land areas of the two ports -compared to free field conditions - is examined by comparing the observed behavior to a widely used lateral spreading prediction empirical equation [85].

2. Performance of Lixouri and Argostoli port structures

2.1. Overview of Lixouri port performance

A satellite image of the Lixouri Port area is shown in Fig. 2. The port area has a length of approximately 0.5 km and the general direction of the waterfront is N–S. The port facilities include the "Davraga" Pier at the north side of the port with an E-W direction, the Main Pier of the port, consisting of a North, Central and South sections, and the Southern Pier also oriented in the E-W direction, at the south side of the port. The port front of Lixouri consists of variable height block-type quay walls (1–4 stacks of blocks) as shown briefly in Fig. 2 and presented in more detail in the Appendix. As discussed in more detail in Section 6, the land area of the port has been reclaimed using building debris (fills) generated from the destructive 1953 earthquakes. The fills of the Lixouri Port area liquefied in the 1st event of the 2014 earthquake doublet and reliquefied in the 2nd event (yellow colored shaded area of the map in Fig. 2). The evidence of liquefaction during the 2nd event was significantly more extensive. Although liquefaction was evident in the first event, it was in the second event that the majority of lateral spreading was observed, whereas in most locations no lateral spreading was observed. For example, in location 5 of Fig. 2, the horizontal displacement was 9 cm and vertical displacement was 6 cm after the first event. After the second event, horizontal and vertical displacements increased to 49 cm and 30 cm, respectively.

The occurrence of soil liquefaction and liquefaction-induced lateral spreading was manifested by coarse-grained sand boils and formation of cracks and displacements towards the free face and has been reported by the GEER Reconnaissance Team (2014) and by a number of other researchers [52,56,57,59–61,79,81]. Example of evidence of coarse-grained sand boils and lateral spreading in Lixouri port is shown in Fig. 2.

In several locations, the ejecta contained significant quantities of gravel as shown in Fig. 2 (photos 1–3). Gravel liquefaction, commonly assumed unlikely, has been observed both in the field and laboratory (see Refs. [39,40]. Liquefaction-induced lateral spreading and

Table 1
Peak values of horizontal ground accelerations (NS/EW) for the two main events of the Cephalonia 2014 earthquake sequence.

Site	Horizontal ground acceleration, a_g (g)	
	1st event (26 Jan 2014)	2nd event (3 Feb 2014)
Lixouri	0.57/0.63	0.61/0.68
Argostoli	0.36/0.43	0.27/0.24
Chavriata	–	0.68/0.77

settlement were also observed in the port area, manifested by soil cracks of variable width that were oriented largely parallel to the port front and at variable distances from the quay wall.

As a result of earthquake shaking, the Lixouri Port quay walls experienced seaward translations that varied between 0.10 m (1.5% of wall height) and 0.45 m (7% of wall height) and rotations between 1.7° and 8.5° depending on the port location. According to Ref. [63] guidelines, the observed level of performance is classified as repairable (case of Argostoli port) to near collapse (case of Lixouri port). Fresh water pipelines running parallel to the back face of the quay walls were also damaged by wall displacement.

2.2. Overview of Argostoli port performance

A satellite image of the Argostoli Port area is shown in Fig. 3. The port area has a length of approximately 1 km and the general direction of the waterfront in the area is NW/ES. The port comprises four main sections, I to IV. Section I (northern section) is used for commercial activities, and the remaining sections for transportation services (loading and unloading of cars and passengers). The port front of Argostoli is supported by block-type quay walls of variable height (two to four stacked blocks in Sections I, II and III, or rubble mound with concrete cap in Section IV), as shown briefly in Fig. 3 and presented in more detail in the Appendix.

Similarly to the Lixouri port, the 2014 earthquakes caused soil liquefaction, sand/gravel ejecta, lateral spreading, settlements and seaward movement of the quay walls. Following the first event, evidence of gravelly boils was observed in the port authority building, but no quay wall movement was observed. Overall, the evidence of liquefaction and movement of the walls were far less pronounced than the Lixouri Port with lateral displacements varying from 10 to 150 cm, as shown in Fig. 3. The operation of the port was largely not disrupted as a result of the earthquake, although some sections of the quay walls particularly in Section I were damaged and isolated. Lateral spreading field measurements were also conducted in the Argostoli Port area and are presented in Section 5.2 of the paper.

3. Strong motion recordings

The two main events of the Cephalonia 2014 earthquake sequence – and the associated aftershocks – were recorded by a number of permanent strong motion instruments of the Hellenic Unified Seismic Network

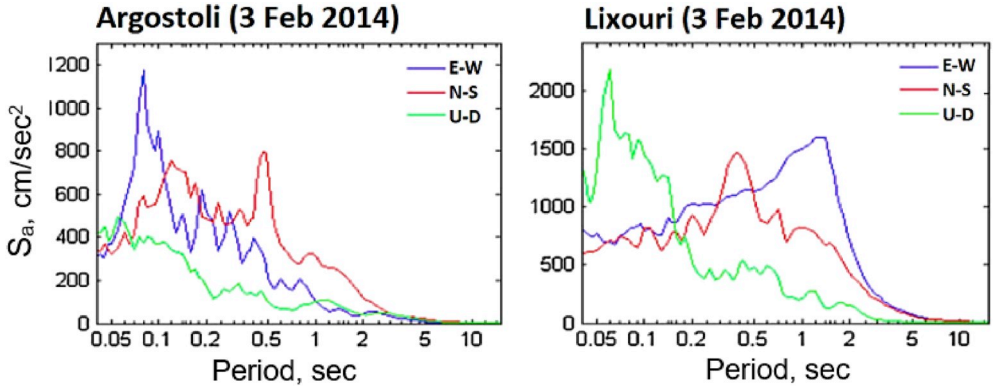

Fig. 4. Acceleration response spectra (three component, elastic, 5% damped) for Lixouri and Argostoli during the 2nd event [79].

Fig. 5. Field measurements of crack widths due to liquefaction-induced lateral spreading in the Cephalonia 2014 earthquakes.

Fig. 6. Location of eight transects surveyed in the Lixouri Port area (with corresponding crack positions), and the accelerograph station which recorded the 2nd event.

(HUSN) and by temporary portable accelerographs installed after the first main event [35,79] Report). The peak values of horizontal ground motions recorded in the meizoseismal area of the earthquakes (Lixouri, Argostoli and Chavriata) are summarized in Table 1.

The peak horizontal ground motion recorded at Chavriata station during the 2nd event is the highest seismic ground acceleration ever recorded in Greece. It is also worth noting that the horizontal ground motion at Lixouri was significantly higher (by 25%–60%) than the motion in Argostoli for both events. The accelerograph stations which recorded the Lixouri and Argostoli ground shaking were located in the vicinity (at distances less than 200 m) from the Port areas of the two towns (see subsequent Fig. 6 and Fig. 7).

The Lixouri E-W acceleration and velocity records – in contrast to the Argostoli ones – are characterized by a strong pulse-like and step-like motion, respectively, an indication of forward directivity [33]. This is illustrated also in the acceleration response spectra at the two sites, shown in Fig. 4, where the acceleration response spectrum for the E-W component of motion in Lixouri is characterized by a peak at periods greater than 1 s.

4. Geological and seismotectonic issues

The bedrock of Cephalonia Island consists of two different carbonitic units: 1) The Pre-Apulian (Paxos) unit (in the western part of the island, consisting of carbonates overlain by marls and perlites (of lower Pliocene age), and 2) The Ionian unit (encountered in the southeastern coastal area of the island) with overlying post-Alpine deposits of Pliocene to Holocene sediments, basal conglomerates, sandstones, marl and conglomeratic alluvial deposits [35] Report [52,78,79]). Locally, the geological structure of the Lixouri area includes lower Pliocene and Pleistocene sediments consisting mainly of basal conglomerate overlain by sandstones and marls. The geological structure of the Argostoli area comprises Pliocene sediments (sandstones, conglomerates, limestones/marly limestones and marls) overlain by marine silty clay soils -with a thickness of 30 m-along the present coastline of the town.

Seismotectonically, Cephalonia is located in the vicinity of the Hellenic Trench in the Ionian Sea (an active plate boundary between the subducting Mediterranean tectonic plate and the overriding Aegean tectonic plate) at the north-westernmost part of the Hellenic Arc. The subduction zone terminates against the Cephalonia Transform Fault (CTF), Fig. 1(a),(b) which plays an important role in Greece's geodynamic and kinematic field. The area has the highest seismicity in Greece with historically documented earthquakes up to M_w 7.2. Historic (1469 to present) seismicity information has been reported by a number of researchers [45,52,53,56,57]; , [2,46,59,62,75].

The location, size and orientation of the causative faults of the Cephalonia 2014 doublet have become the subject of continuing research by many investigators during the last few years [11,12,19,31, 44–46,51,53,59,69,70,74,81] applying a wide range of methodologies (e.g. continuous GPS measurements and differential SAR interferometry). Although the proposed fault models are not identical, a consensus exists that the causative faults of the two main events are on-shore dextral strike-slip faults (with a small dip-slip component) located in the Paliki peninsula of Cephalonia at a sub-parallel orientation to the CTF.

An understanding of the causative fault characteristics is needed to

Fig. 7. Location of the sixteen transects surveyed in the Argostoli Port area (with corresponding crack positions), and the accelerograph station which recorded the 2nd event.

Table 2
Measured values of crack widths and cumulative horizontal displacements along eight transects in the Lixouri Port area (including few vertical crack offset measurements).

Point	Distance from face, L (m)	Height of free face, H (m)	Crack width/ Vertical offset, (cm)	Cumulative Lateral Spreading Displacement, (cm)
TRANSECT -1				
A1	45.00	4.25	0.10	0.10
B1	35.00	4.25	2.50/3.00	2.60
C1	32.00	4.25	2.50	5.10
D1	23.00	4.25	4.00	9.10
E1	17.00	4.25	2.50	11.60
F1	6.00	4.25	1.50	13.10
G1	2.00	4.25	30.00	43.10
TRANSECT - 2				
A2	69.20	4.60	0/0.50	0
B2	41.45	4.60	0.50	0.50
C2	29.80	4.60	1.50	2.00
D2	27.10	4.60	0.50	2.50
E2	18.10	4.60	12.00	14.50
F2	11.10	4.60	4.00	18.50
G2	5.20	4.60	1.00	19.50
H2	0.80	4.60	35.00/18.00	54.50
TRANSECT - 3				
A3	91.20	7.60	0	0
B3	57.40	7.60	0.50	0.50
C3	42.85	7.60	1.00	1.50
D3	33.10	7.60	2.50	4.00
E3	26.54	7.60	1.00	5.00
F3	21.00	7.60	6.00	11.00
G3	16.30	7.60	4.00	15.00
H3	4.80	7.60	0	15.00
TRANSECT - 4				
A4	89.70	7.60	0	0
B4	69.30	7.60	0.50	0.50
C4	39.17	7.60	2.00	2.50
D4	24.38	7.60	1.50	4.00
E4	19.72	7.60	3.00	7.00
F4	17.62	7.60	3.00	10.00
G4	10.47	7.60	1.50	11.50
TRANSECT - 5				
A5	81.80	4.33	0.10	0.10
B5	72.20	4.33	0.10	0.20
C5	41.25	4.33	1.00	1.20
D5	23.80	4.33	3.50	4.70
E5	17.75	4.33	4.00	8.70
F5	13.64	4.33	6.50	15.20
G5	9.00	4.33	5.00	20.2
H5	3.37	4.33	100.00	120.2
TRANSECT - 6				
A6	88.20	4.33	1.00	1.00
B6	73.60	4.33	0	1.00
C6	44.50	4.33	0.20	1.20
D6	34.50	4.33	3.00	4.20
E6	28.30	4.33	2.00	6.20
F6	25.70	4.33	1.00	7.20
G6	22.90	4.33	10.00	17.20
H6	15.40	4.33	6.00	23.20
I6	9.64	4.33	3.00	26.20
J6	5.13	4.33	49.00/30.00	75.20
TRANSECT - 7				
A7	70.00	2.60	0.20	0.20
B7	66.00	2.60	1.50	1.70
C7	29.50	2.60	0.50	2.20
D7	26.60	2.60	2.00/4.00	4.20
E7	22.20	2.60	4.00	8.20
F7	20.75	2.60	5.50	13.70
G7	16.32	2.60	2.00	15.70
H7	14.85	2.60	6.00	21.70
I7	8.80	2.60	20.00	41.70
J7	4.50	2.60	110.00	151.70
TRANSECT - 8				
A8	32.70	2.60	0.30	0.30
B8	8.00	2.60	2.50	2.80
C8	5.90	2.60	1.50	4.30

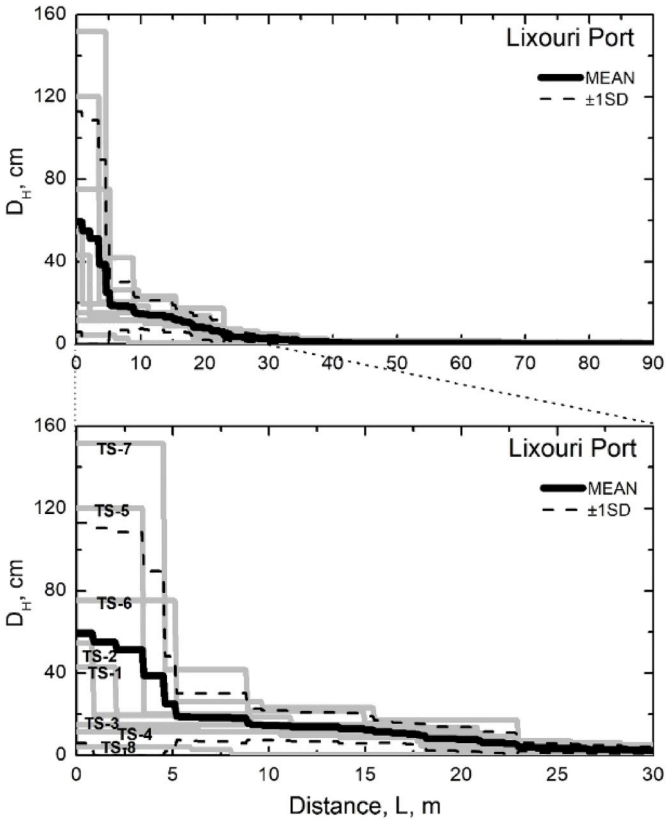

Fig. 8. Distribution of measured cumulative lateral spreading displacements, along with mean and mean ±1S.D curves, in the Lixouri Port area.

use the [85] model predictions presented subsequently. The fault model proposed by Ref. [74] is used, as shown in Fig. 1(a),(b) to estimate lateral spreading displacements. According to this model (Fig. 1(a)) the causative fault of the 1st event (26 Jan 2014) is identified as a strike-slip fault having a strike of 20°, a dip of 80°, and a rake of 180° with a hypocentral depth of 8 km. The fault rupture propagated up-dip from the hypocenter, reaching a shallow depth and continued along strike (in NE direction).

For the 2nd event (3 Feb 2014) (with a hypocentral depth of 5 km) the model comprises the two fault segments shown in Fig. 1(b), which ruptured almost simultaneously. The rupture of segment #1 (characterized by strike/dip/rake angles of 180°/86°/147°) originated at shallow depth and propagated mainly southward towards the town of Lixouri. The rupture of segment #2 (characterized by strike/dip/rake angles of 33°/76°/164°) followed unilateral southward direction. It should be noted that the segment #1 of the fault is in close proximity to the town of Lixouri and therefore the southward rupture propagation is consistent with the forward directivity characteristics of the motion recorded during the 2nd event by the Lixouri accelerograph station.

5. Measurement of quay wall and fill displacements

Quay walls at ports subjected to a seismic excitation may experience transient (during the earthquake) and permanent (after the earthquake) lateral displacements and rotations due to two primary, but also interacting, mechanisms [1,72]:

(a) an outward seismic wall movement due to the seismic shaking, which is a complex soil-structure interaction problem and is a function of the quay wall geometric (and inertial) characteristics, fill properties and shaking characteristics; and
(b) liquefaction induced lateral ground movement.

Table 3
Measured values of crack widths and cumulative horizontal displacements along sixteen transects in the Argostoli Port area (including few vertical crack offset measurements).

Point	Distance from face, L (m)	Height of free face, H (m)	Crack width/ Vertical offset (cm)	Cumulative Lateral Spreading Displacement (cm)
TRANSECT – 1				
A1	37.80	6.50	1.00	1.00
B1	22.80	6.50	0.20	1.20
C1	17.30	6.50	0.30	1.50
D1	9.50	6.50	0.50	2.00
E1	0.80	6.50	1.00	3.00
TRANSECT – 2				
A2	42.10	6.50	1.00	1.00
B2	36.60	6.50	1.00	2.00
C2	29.00	6.50	0.50	2.50
D2	18.20	6.50	1.00	3.50
E2	12.00	6.50	1.00	4.50
TRANSECT – 3				
A3	51.10	6.50	1.50	1.50
B3	45.70	6.50	0	1.50
C3	27.80	6.50	0.70	2.20
D3	15.80	6.50	0.30	2.50
E3	1.85	6.50	1.00	3.50
TRANSECT – 4				
A4	30.78	3.00	0.70	0.70
B4	25.75	3.00	2.50/3.00	3.20
C4	21.96	3.00	0.70	3.90
D4	13.02	3.00	1.20	5.10
E4	11.36	3.00	3.00	8.10
F4	4.08	3.00	3.00	11.10
G4	1.90	3.00	2.30	13.40
TRANSECT – 5				
A5	17.68	3.00	0.50	0.50
B5	12.55	3.00	3.00	3.50
C5	7.84	3.00	0.50	4.00
D5	0.52	3.00	6.50/11.00	10.50
TRANSECT – 6				
A6	11.38	3.00	2.00	2.00
B6	9.88	3.00	2.00	4.00
C6	2.03	3.00	5.00/5.50	9.00
TRANSECT – 7				
A7	9.33	2.50	5.00	5.00
B7	3.46	2.50	4.00/3.00	9.00
TRANSECT – 8				
A8	9.72	2.50	1.50	1.50
B8	8.62	2.50	0.30	1.80
C8	4.44	2.50	3.00/2.70	4.80
TRANSECT – 9				
A9	12.00	2.50	3.00	3.00
B9	9.51	2.50	1.70	4.70
C9	0.59	2.50	5.50/3.00	10.20
TRANSECT – 10				
A10	11.54	2.50	3.50	3.50
B10	2.11	2.50	4.00	7.50
TRANSECT – 11				
A11	12.56	2.50	1.80	1.80
B11	3.37	2.50	2.50	4.30
TRANSECT – 12				
A12	33.34	2.50	2.50	2.50
B12	29.36	2.50	0.50	3.00
C12	11.80	2.50	1.50/2.30	4.50
D12	1.75	2.50	4.00	8.50
TRANSECT – 13				
A13	36.90	2.50	0.50	0.50
B13	36.10	2.50	4.00	4.50
C13	29.44	2.50	0.70	5.20
D13	16.12	2.50	1.00	6.20
E13	4.69	2.50	2.50	8.70
F13 1	1.03	2.50	3.00	11.70
TRANSECT – 14				
A14	38.85	2.50	0.30	0.30
B14	37.72	2.50	0.80	1.10
C14	36.40	2.50	1.00	2.10
D14	20.08	2.50	1.90	4.00
E14	11.27	2.50	1.20	5.20
F14 1	2.86	2.50	5.00/9.00	10.20
TRANSECT – 15				
A15	21.09	0.80	1.50	1.50
B15	17.66	0.80	0.90	2.40
C15	14.77	0.80	0.50	2.90
D15	9.50	0.80	0.70	3.60
E15	2.35	0.80	16.00/5.00	19.60
TRANSECT – 16				
A16	21.66	0.80	0.20	0.20
B16	17.52	0.80	0.30	0.50
C16	15.38	0.80	1.00/1.50	1.50
D16	8.48	0.80	0.20	1.70
E16	6.44	0.80	1.00	2.70
F16	1.76	0.80	3.00/5.50	5.70

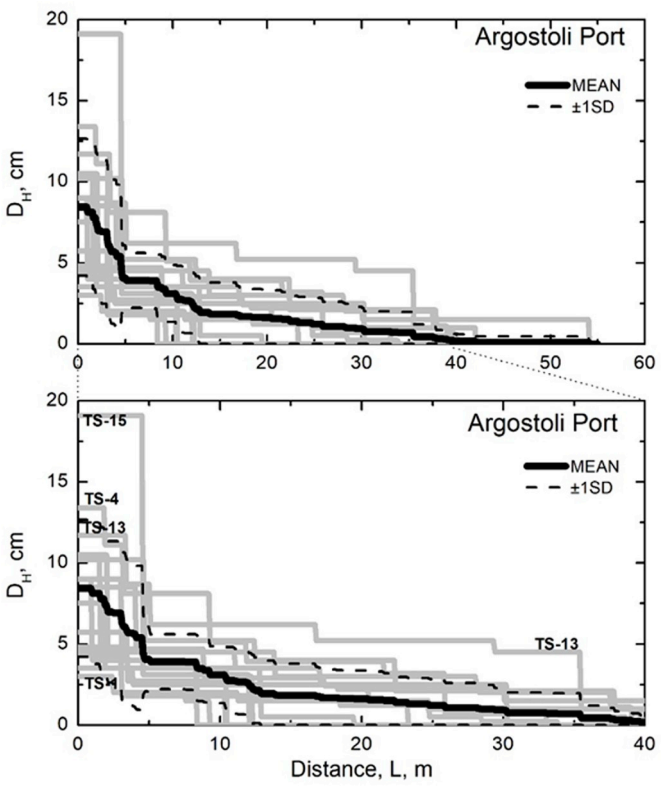

Fig. 9. Distribution of measured cumulative horizontal displacements in Argostoli Port, along with mean and mean ±1S.D curves.

Liquefaction-induced lateral spreading of ground is presently recognized as a major cause of damage to buildings and civil infrastructure (roadways, embankments, bridges, dams, pipelines and harbor facilities) [17,23,47] [18]. The pore pressure increase and associated reduction of shear resistance due to liquefaction results in lateral displacement of gently sloping surficial ground or of level ground in the vicinity of a free face to a water body. Quay walls represent a special case of lateral spreading in the vicinity of a free face.

Depending on soil properties, site morphology [7], continuity of liquefiable layers [68] and earthquake characteristics, the amount of lateral ground displacement – which has also been found to be related to ground settlement [72] – may range from a few centimeters to several meters and constitutes a serious hazard to structures supported by the

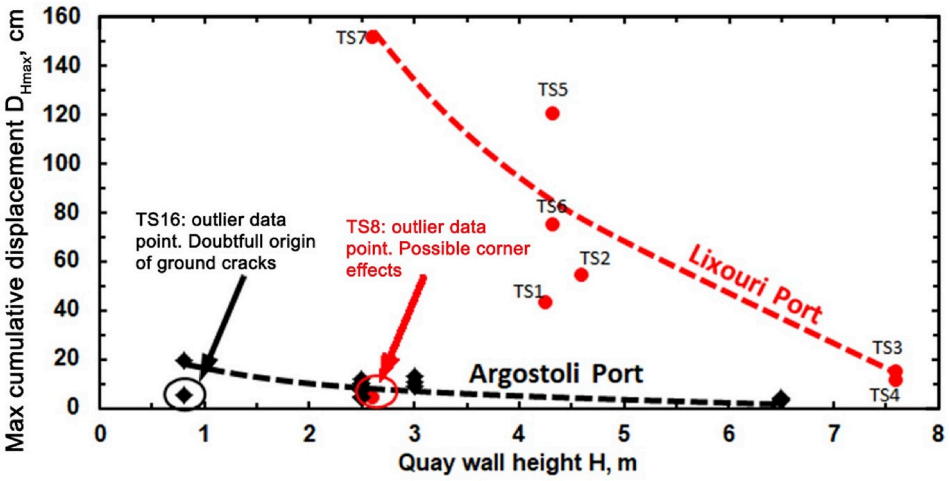

Fig. 10. Dependence of observed maximum cumulative lateral displacement on the quay wall height.

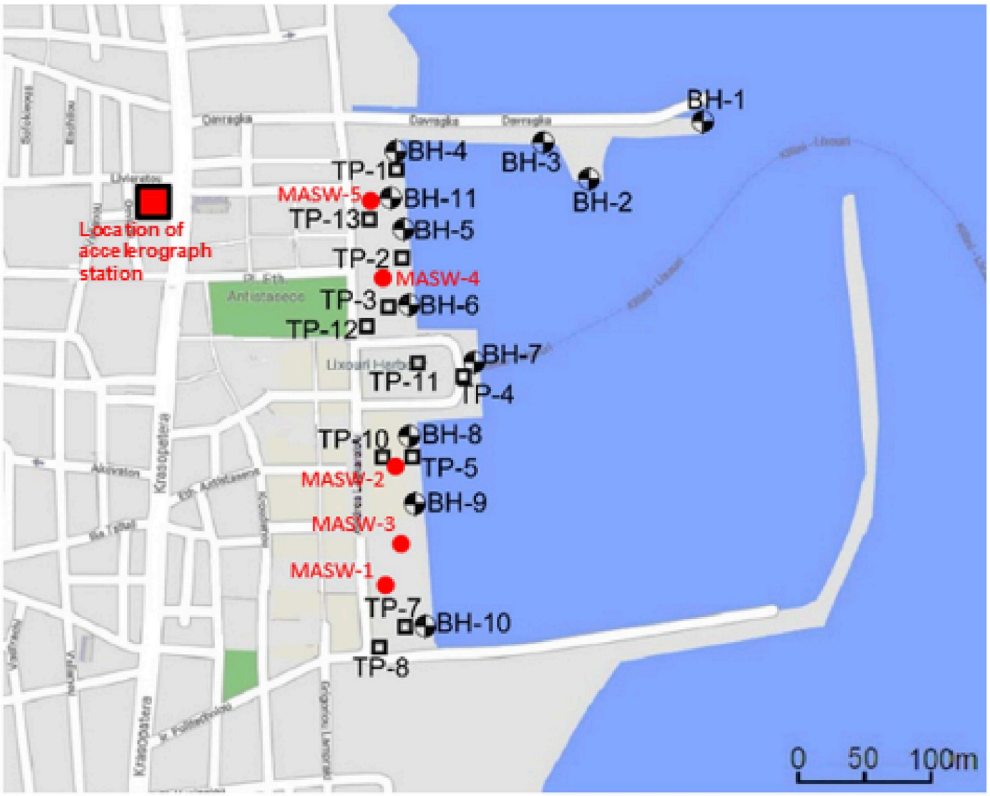

Fig. 11. Location of boreholes, test pits, MASW measurements and acceleration station in the Lixouri Port area.

moving ground [1] The damaging potential of lateral spreading to the affected structures - as well as the extent of damage - depends mainly on the amount of lateral displacements. Moriarty [54] used the following relation between magnitude of lateral spreading and damage potential: ≥100 cm → Very High, 30 cm–100 cm → High, 10 cm–30 cm → Moderate and ≤10 cm → Low. It is therefore critical to be able to reliably assess the expected magnitude of lateral ground spreading displacements [3,80].

Empirical methods to predict the magnitude of lateral spreading under free-field conditions (i.e. methods not based on a mechanistic model of the process) appeared first in the 1980s [38] and are still widely used in professional practice, currently associated with probabilistic approaches in the performance-based framework [30]. The empirical methods are based on Multilinear Regression Analysis (MLR) of datasets derived from case histories of measured lateral ground displacements in a number of earthquakes at different parts of the world - also including cases with negligible displacements - [6,37,65,85,89,90]. The accuracy of the empirical methods of lateral spreading prediction ranges between 2 and 0.5 times the measured values [80]. The accuracy has reportedly improved using soft computing techniques for processing data from field measurements, involving the use of optimization techniques, e.g. Artificial Neural Networks (ANN) and Genetic Programming (GP) [10,42,73], as well as performance-based approaches [26]. The available databases on measured liquefaction-induced lateral spreading, especially in the land areas behind quay walls of ports, have also recently expanded following a number of strong recent earthquakes,

Fig. 12. Location of boreholes, test pits, MASW measurements and acceleration station in the Argostoli Port area.

(Kaikoura, New Zealand, 2016; Muisne, Ecuador, 2016; Iquique, Chile, 2014) as reported in pertinent GEER Reports and other literature.

Semi-empirical methods of lateral spreading analysis have also been developed. These utilize observed ground performance in association with the assumption of a simplified mechanism of the phenomenon, e.g. Ref. [88]. Other available methods for analyzing lateral spreading include (a) the utilization of Newmark's sliding block approach [49,58], (b) numerical analyses [27,28,36,82,83] and (c) physical modeling or full scale testing, either under 1-g gravity conditions or in multi-g centrifuges [24,25,29,43,50,71,76,77].

In this paper, results of lateral spreading measurements in the Port areas of Lixouri and Argostoli - performed after the 2nd main event - are presented using procedures similar to the ones reported by Refs. [20–22, 41,67]. The lateral spreading measurements were conducted by ground surveys (i.e. by direct field measurements) using tape measurements of crack widths (as shown in Fig. 5).

Other methods for such measurements have also been used by others, including the use of aerial photographs and geodetic measurements, whereas the capabilities of advanced methods such as Light Detection and Ranging (LiDAR), satellite image pair correlations, digital photogrammetry and ground-based or UAV (drone) - mounted surveys have also been recently demonstrated [15,22,64,66,86,87].

The measurements presented in this paper involved records of crack widths along a number of transects oriented in a direction perpendicular to the line of multi-block quay walls. The inland horizontal distance, L, of each crack from the free face (seaward face of quay wall) was also recorded for all transects. The location of eight transects (TS-1 to TS-8) surveyed in the Lixouri Port area are depicted in Fig. 6. The location of the 16 transects surveyed in the Argostoli Port area are shown in Fig. 7. The results of measurements in the two port areas are discussed in the following two subsections.

5.1. Displacement measurements in the Lixouri Port area

The results of measurements along the 8 transects surveyed in the Lixouri Port area are summarized in Table 2, including the geometric characteristics of each transect, the measured width of ground cracks, the corresponding horizontal distance from the free face, and the cumulative displacement. Table 2 also includes the results of measurements of vertical offset between the two edges of a number of cracks, which were found to range from 3 cm to 30 cm. The distance of the Lixouri Port area from the causative fault, R, is approximately equal to 2 km (Fig. 1(b)) and the peak recorded horizontal ground acceleration (at a distance of 200 m from the seafront) is 0.68 g (E-W) (Table 1). The recorded E-W component of the strong motion at the Lixouri Port exhibits the characteristics of forward directivity, whose effect on the lateral ground spreading mechanism has not yet been investigated, but is possible to have played a role in the total permanent displacement and rotation of the quay walls.

The distributions of cumulative horizontal ground displacement, D_H, vs. distance from the free face, L, along the 8 transects (TS-1 to TS-8) surveyed at the Lixouri Port area are shown in Fig. 8. The plots indicate that small ground displacements occurred up to a distance of 90 m behind the quay wall, although the majority of lateral ground movement occurred within a distance of only 30 m. Lateral displacement at the back face of the quay walls ranged from a few centimetres (4.3 cm) to

Fig. 13. View of test pit TP-2 operations and excavated material in Lixouri port.

152 cm for the eight transects. The pattern of ground movements is of the "block-type" (i.e., defining a block of fill behind the wall) for small inland distances (<5 m) and of "distributed type" for larger distances. It should be noted that the field surveys of ground crack widths behind the quay walls, included the width of the gap formed between the back face of the quay wall and the backfill. The width of this gap may in some cases also include - in addition to lateral ground movement - the lateral displacement of the top of the quay wall, caused by translation and rotation. It is therefore necessary to emphasize that the maximum lateral displacements (i.e. for a horizontal distance L = 0 m) shown in Fig. 8 will, in some transects, include the seaward horizontal displacement of the corresponding quay wall.

The D_H vs. L curves shown in Fig. 8 correspond to different transects and are characterized by significant variability. The plots include the mean curve and also curves for ±1SD. Such a variability should be expected given: (1) the varying heights of free face (2.6 m–7.6 m), and the different number of stacked concrete blocks that form the quay wall; (2) possible variations of subsurface conditions in the port area, and (3) the presence of physical restraints to lateral ground movement of quay walls (e.g. the concrete ramps used by the Ferries servicing the Port of Lixouri for docking and loading/unloading cars). These differences in conditions are considered in Section 7 of the paper, in which the measured values of lateral movements are compared to empirically predicted values of lateral spreading.

5.2. Displacement measurements in the Argostoli Port area

The results of crack width measurements along 16 surveyed transects (TS-1 to TS-16) in the Argostoli port are summarized in Table 3 and the corresponding cumulative horizontal displacements are shown in Fig. 9. Table 3 also includes measured values of vertical offset between the two edges of a number of cracks, which were found to range from 1.5 cm to 11 cm. The distance of the Argostoli Port area from the causative fault is 7 km whereas the peak recorded horizontal ground acceleration is 0.24 g (E-W) (Table 1).

As shown in Fig. 9, the lateral spreads in the Argostoli Port area extended to a distance of ~55 m behind the quay walls, although the cumulative lateral movement remained less than 1 cm for inland distances larger than 40 m. The plots of Fig. 9 indicate that the maximum horizontal displacement in the Argostoli Port along the 16 surveyed transects, ranged from 3.5 cm to 20 cm (about an order of magnitude lower than the Lixouri Port area). This should be expected given the larger distance (7 km) of the Argostoli Port area from the causative fault compared to the Lixouri Port area, as well as the lower peak value of recorded ground acceleration (0.24 g compared to 0.68 g).

As shown in Figs. 8 and 9, the measured displacements have higher variability in the vicinity of the free face. Assuming that the maximum value of cumulative lateral displacement, D_{Hmax}, for each transect is mainly affected by the height of free face, H, it is possible to plot average D_{Hmax} vs. H curves for the two port areas (Lixouri and Argostoli) as shown in Fig. 10. The plots of Fig. 10 indicate that (a) the cumulative lateral displacements at the Lixouri port were at least one order of magnitude higher compared to the Argostoli Port (as already mentioned) and (b) the cumulative displacement strongly depends on the height of the free face, i.e. the higher the quay wall, the lower the corresponding lateral spreading. This behavior may be explained by the higher lateral resistance offered by the higher and heavier multi-block quay walls.

6. Geotechnical data

A soil exploration study was undertaken at the Ports of Lixouri and Argostoli, following the 2014 Cephalonia earthquakes, with the goal to obtain data for retrofitting the laterally displaced and tilted quay walls

Fig. 14. View of test pit TP-1 operations and excavated material in Argostoli port.

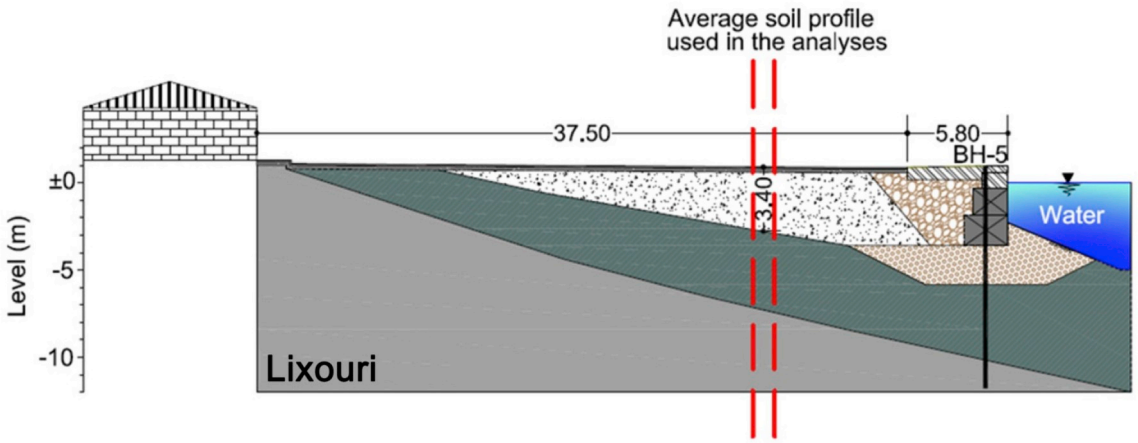

Fig. 15. Average cross section at the Lixouri Port area.

of the port areas. The exploratory borings were advanced through the concrete blocks of the quay walls to the underlying natural soil formations whose mechanical properties were evaluated by laboratory testing on "undisturbed" samples.

Eleven borings (BH-1 to BH-11) with depths up to 20 m were drilled at the Lixouri Port (Fig. 11) in March 2014, and nine borings (BH-1 to BH-9) with depths up to 17 m in April 2016 at the Argostoli Port (Fig. 12). The exploration program did not include, however, any borings through the reclaimed land areas of the two ports; thus, no data are available regarding the thickness and mechanical properties of the fills used for reclaiming and expanding the land areas of the ports, following the destructive Cephalonia earthquakes of 1953.

The nature of the fills was characterized primarily using test pits. In total 13 large test pits were excavated in Lixouri and another 6 test pits were excavated in Argostoli using a backhoe at small distances from the back face of the quay walls. The test pits were of relatively large size (a couple of meters in width and length) and extended to depths below the water table reaching 2.3 m. Characteristic photos are shown in Fig. 13 for Lixouri and Fig. 14 for Argostoli. The material encountered in all test pits in both ports was visually similar. It included, as shown in the figures, large corestones (commonly 10–60 cm) that were part of the collapsed masonry buildings in a matrix of finer debris that included gravels, sands and low plasticity silts. Disturbed samples of the debris were collected from the test pits and laboratory tests were conducted.

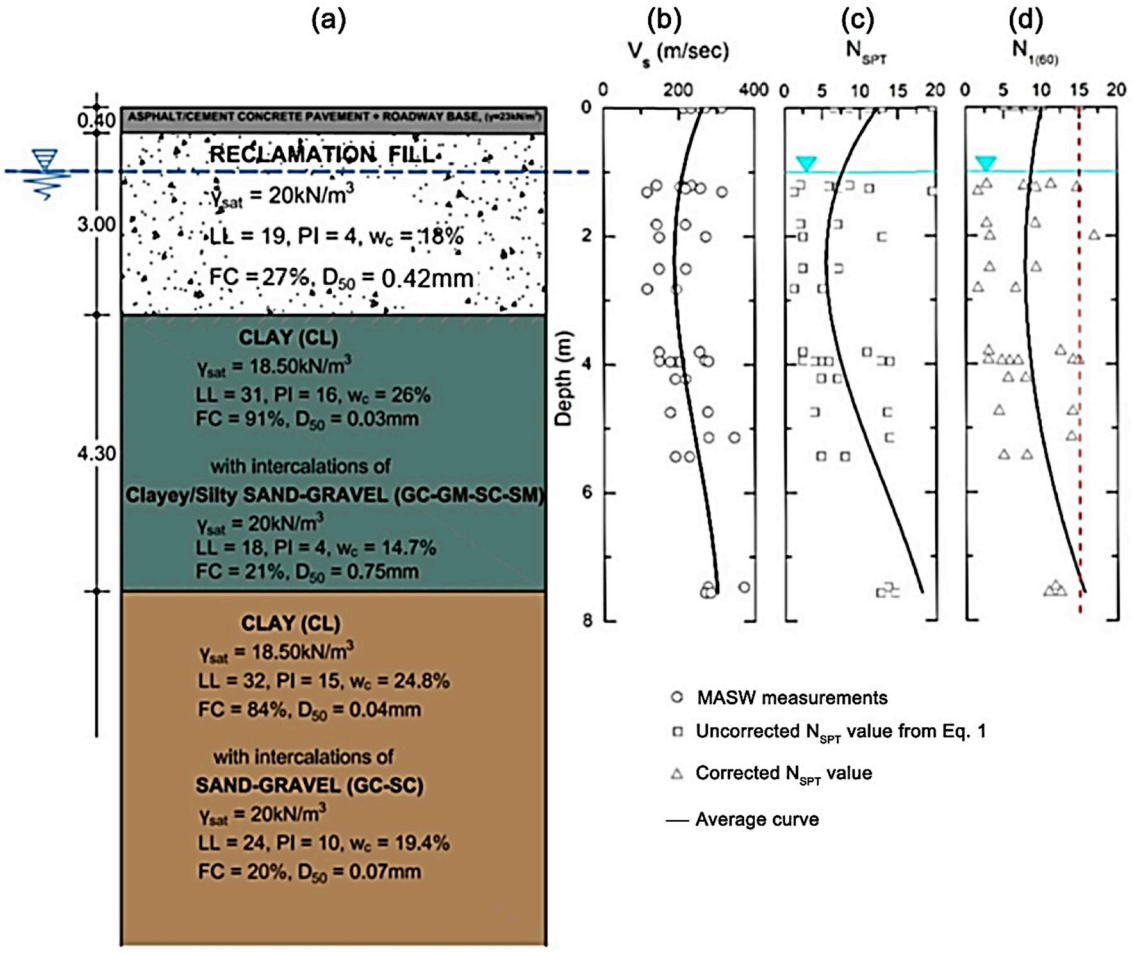

Fig. 16. (a) Average 1-D soil profile of the Lixouri Port land area, (b) measured values of V_s from MASW test, (c) computed values of uncorrected N_{SPT} (from Eq. (1)) and (d) corrected N_{SPT} values [9,13].

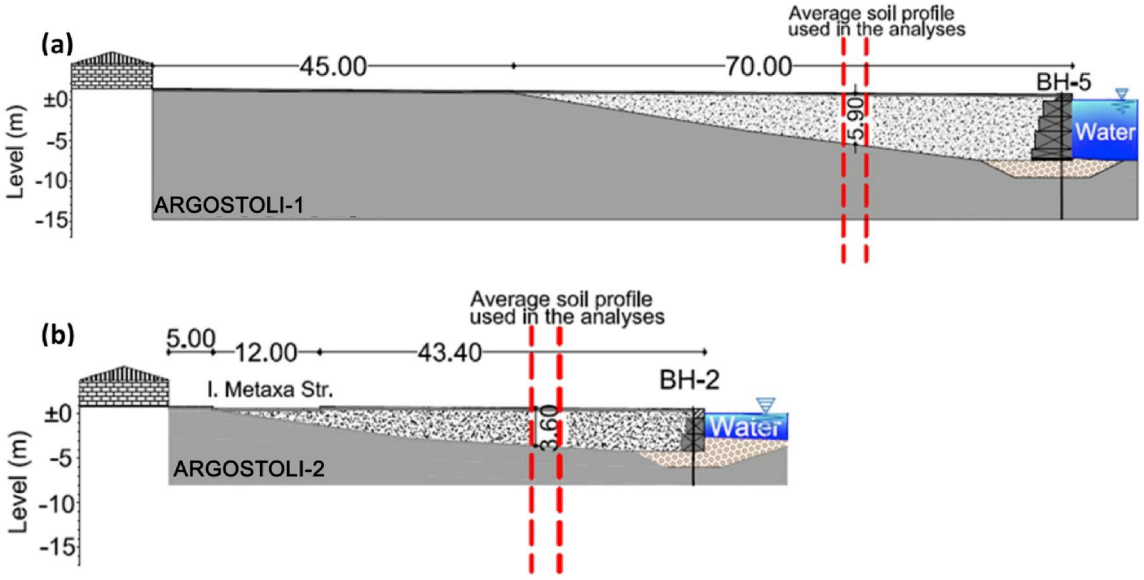

Fig. 17. Average cross-sections of the Argostoli Port area (a) Argostoli-1 (North area), (b) Argostoli-2 (South area).

The following average physical and index properties of the reclamation fills were derived: $\gamma_{sat} = 20$ kN/m^3, LL = 19, PI = 4, w = 18%, FC = 27%, and $D_{50} = 0.42$ mm.

Based on the extrapolation of soil stratigraphy found from the exploratory borings, data from test pits, the local geological conditions, and eyewitnesses accounts (regarding the reclamation history and

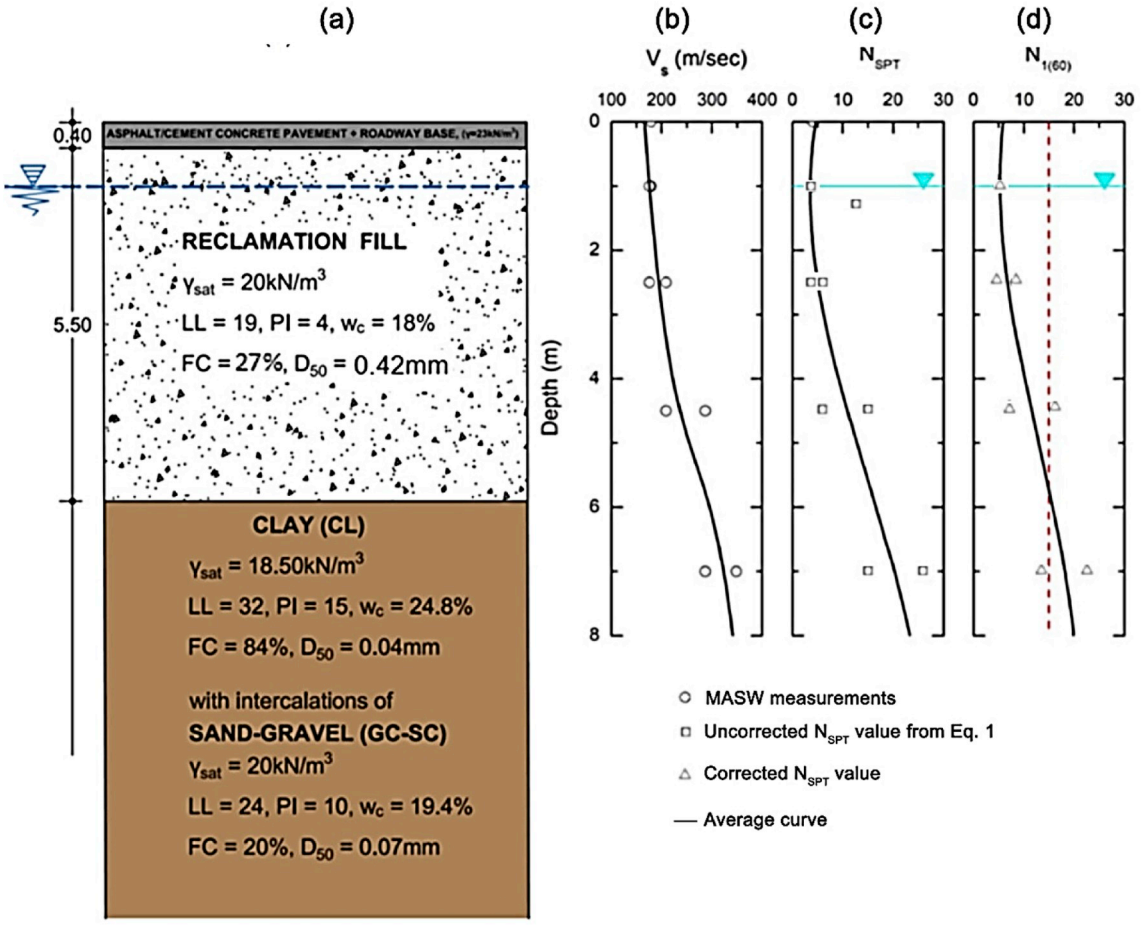

Fig. 18. (a) Average 1-D soil profile of the Argostoli-1 Port land area, (b) measured values of V_S from MASW test, (c) computed values of uncorrected N_{SPT} (from Eq. (1)) and (d) corrected N_{SPT} values [9,13].

expansion of the Port areas following the destructive Cephalonia earthquakes of 1953), a typical 2-D cross-section of the Lixouri Port was established and is shown in Fig. 15. As indicated in the figure, subsurface stratigraphy of the Lixouri port consists of a surficial layer of artificial reclamation fill. These fills are primarily debris from collapsed structures following the 1953 earthquake and are underlain by an alluvial layer of variable thickness (CL) with intercalations of GC-GM–SC–SM, that extends inland up to the coastal roadway. The physical, index, and mechanical properties of this layer were estimated from laboratory testing and their average values are included in the 1-D cross-section of Fig. 16. This layer is underlain by a cohesive formation with sand-gravel intercalations, extending to the maximum investigated depth. The physical, index, and mechanical properties of this layer were also estimated from laboratory testing with average values included in the 1-D cross-section of Fig. 16.

Surface wave measurements using the MASW technique shared by Ref. [5] allowed the evaluation of shear wave velocity vs. depth profiles in the two port areas, which (for the case of Lixouri Port) are plotted in Fig. 16. The lack of N_{SPT} data for the land area of the ports, made it necessary to indirectly evaluate N_{SPT} – depth profile by utilizing the correlation (shown in Eq. (1)) developed using Greek data by Ref. [4]. The reliability of the above empirical V_s -N_{SPT} correlation has been validated by Refs. [4,8]:

$$V_S\left(\frac{m}{\sec}\right) = 107.6 N_{SPT}{}^{0.36} \Rightarrow N_{SPT} = \left(\frac{V_S}{107.6}\right)^{2.78} \quad (1)$$

where: N_{SPT} = uncorrected value of SPT blow count.

The empirically derived N_{SPT} – depth profile for Lixouri Port is also included in Fig. 16 indicating low values of N_{SPT} (≈5).

Corresponding data for the Argostoli Port area were obtained and utilized to establish two approximate, representative cross sections: Argostoli −1 (north area of the port) and Argostoli – 2 (south area of the port), shown in Fig. 17. Approximate 1-D geotechnical sections for the two locations of Argostoli Port area are shown in Fig. 18(a) and Fig. 18 (b) along with pertinent V_S – depth and N_{SPT} – depth profiles.

The approximate geotechnical V_S - N_{SPT} profiles shown in Figs. 18 and 19 are used in the following section to compare the measured lateral displacement with lateral spreading estimates predicted by the empirical model of [85] for free-field conditions.

7. Measured lateral spreading magnitudes VS. Empirical predictions under free field conditions

The importance of soil liquefaction/lateral spreading case history data for developing improved predictive empirical, analytical or numerical methods has been repeatedly emphasized in recent publications [17,47]. At present, the available empirical methods for predicting the magnitude and spatial distribution of liquefaction-induced lateral spreading have been derived based on data obtained in free-field ground conditions. In this respect the lateral spreading measurements performed in the Lixouri and Argostoli Ports following the 2014 Cephalonia earthquake doublet constitute a valuable dataset which can be utilized to investigate the capacity of the quay walls to reduce the development of lateral spreads during earthquake shaking.

The [85] empirical relation, which is widely used in practice for predicting the magnitude of liquefaction-induced lateral spreading under free field conditions, is used and compared with the measured

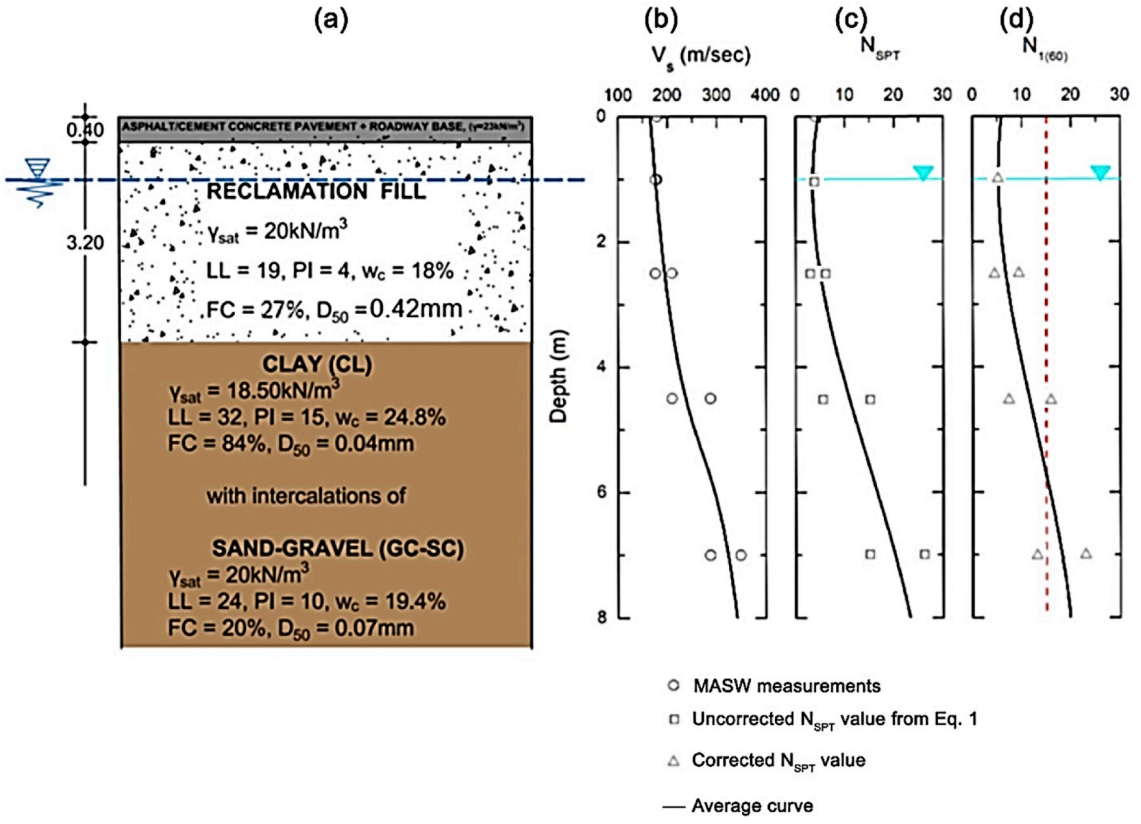

Fig. 19. (a) Average 1-D soil profile of the Argostoli-2 Port land area, (b) measured values of V_S from MASW tests, (c) computed values of uncorrected N_{SPT} (from Eq. (1)) and (d) corrected N_{SPT} values [9,13].

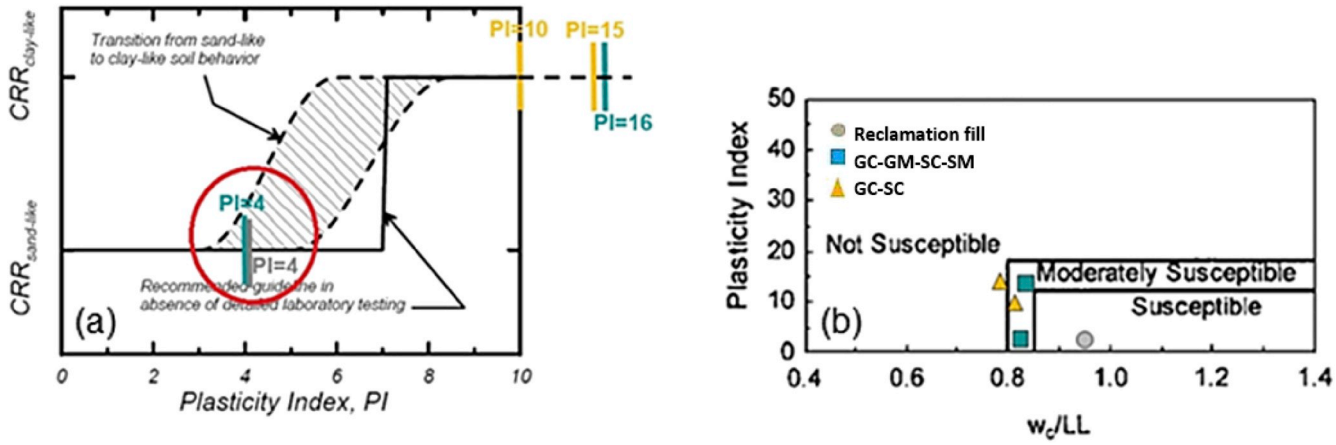

Fig. 20. (a) Behavior of soil materials encountered at the Lixouri and Argostoli Port land areas based on the recommended guideline by [14], (b) Liquefaction susceptibility of fine-grained materials encountered in the Lixouri and Argostoli Port land areas based on [16].

values in the port areas. The [85] relation for the case of level ground with a free face, is shown in Eq. (2):

$$Log\, D_H = -16,713 + 1,532M - 1,406 Log R^* - 0,012R + 0,592 LogW + 0,540 LogT_{15} + 3,413 Log(100 - F_{15}) - 0,795 Log(D50_{15} + 0,1mm) \quad (2)$$

where:

D_H estimated lateral ground displacement, in meters.
M moment magnitude of the earthquake
R* modified source distance $R^* = R_o + R$, where R_o a distance constant that is a function of earthquake magnitude, M, $R_o = 10^{(0.89M - 5.64)}$
R nearest horizontal or map distance from the site to the seismic energy source, in kilometers
W free-face ratio defined as the height, H, of the free face divided by the distance, L, in percent
T_{15} cumulative thickness of saturated granular layers with corrected blow counts, $(N_1)_{60}$, less than 15, in meters.
F_{15} average fines content, or fraction of sediment sample passing a No. 200 sieve for granular materials included within T_{15}, in percent

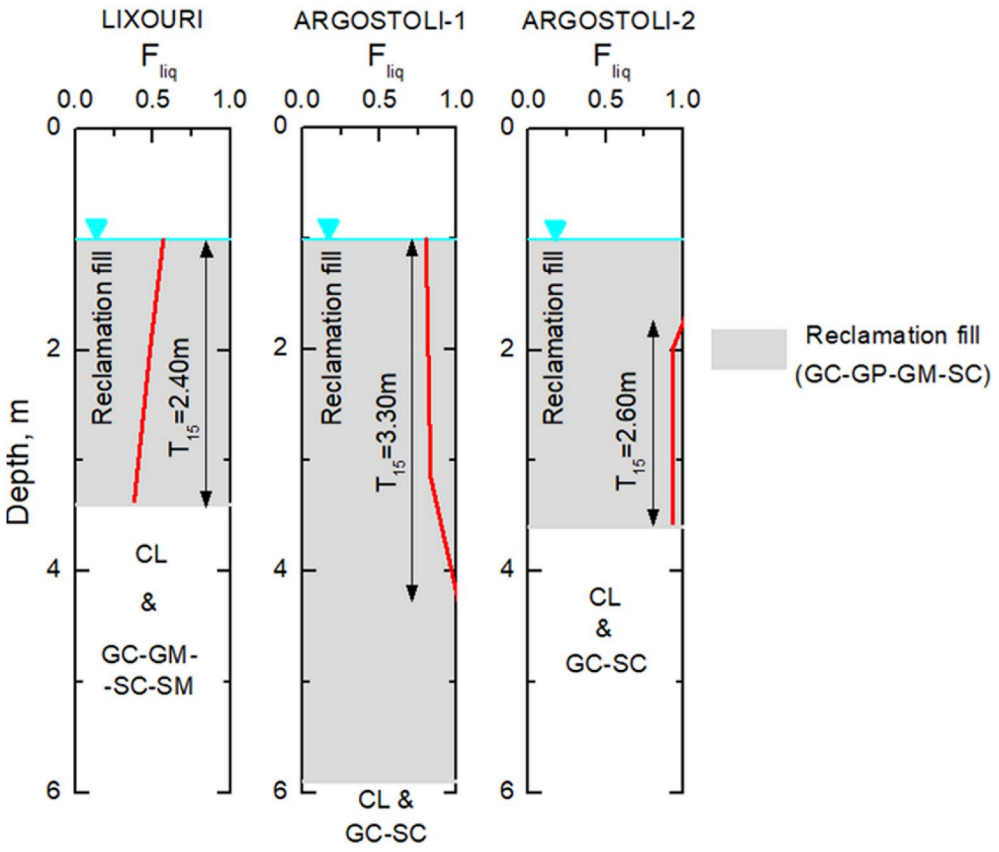

Fig. 21. Variation of F_{liq} with depth in the layer of reclamation fill for the average soil profiles of Lixouri. Argostoli-1 and Argostoli-2.

$D50_{15}$ average mean grain size for granular materials within T_{15}, in millimeters, from the base of the free face to the point in question, in percent.

The input parameters of Eq. (2) for the [85] relation belong in three categories: (a) earthquake characteristics (magnitude and distance from the causative fault, (b) geometric characteristics (height of free face and horizontal inboard distance, and (c) soil characteristics (thickness of liquefied layer and average values of fines content and mean grain size). The predictions of Eq. (2) – on the basis of comparisons with measured values of lateral ground displacements – have been found to deviate, in general, from +200% to −50% from the observed values.

By applying the liquefaction susceptibility criteria recommended by Refs. [14,16] (as shown in Fig. 20) to the representative soil conditions of the Lixouri and Argostoli port areas, it becomes evident that the most liquefaction–susceptible soil materials are the reclamation fill and the intercalations of coarse-grained materials which are interbedded in the underlying cohesive layers. The horizontal continuity of the coarse-grained intercalations, as well as their minimum thickness (which is a prerequisite for incorporating them into the thickness of liquefied layer, e.g. Refs. [17,48,55,84] is highly uncertain, and for this reason only the reclamation fill material is considered as liquefiable in the subsequent liquefaction analyses.

For the identified liquefiable layer, liquefaction triggering analysis was performed for the Lixouri Port area (Lixouri) and the two characteristic profiles of Argostoli Port area (Argostoli-1 and Argostoli-2), following the procedure recommended by Ref. [13]. The results of the analyses for the three sites, in the form of Safety Factor against liquefaction, F_{liq}, are shown in Fig. 21, indicating that the thickness of the liquefied layers, T_{15}, at the three sites is 2.4 m for the Lixouri site, 3.3 m for Argostoli-1 and 2.6 m for Argostoli-2. It is recognized that these thicknesses of liquefied layers are somewhat uncertain, given the limited subsurface data. As shown in Figs. 16(d), 18(d) and 19(b) the corrected values of SPT blow count $(N_1)_{60}$ in the liquefied layers are lower than the critical value ($(N_1)_{60} = 15$) adopted in the [85] empirical relation.

In the following two subsections the predicted magnitudes of lateral spreading at the two port areas are presented by applying the [85] equation using the following values of input parameters: $T_{15LIX} = 2.4$ m, $T_{15ARG} = 3.3$ m/2.6 m, $D50_{15} = 0.42$ mm, $F_{15} = 27\%$, $M_w = 6$, and $R_{LIX} = 2$ km, $R_{ARG} = 7$ km. It must be noted that the $D50_{15}$ and F_{15} values represent average estimates of the average grain size and fines content of the liquefiable fills, but variation in the data was observed. In addition, these estimates are based on samples of the fills that do not include the large corestones that are part of the debris. The role of these large corestones in the field response is not yet well understood. Including them in the grain size distribution would result in a significantly higher average grain size distribution (and smaller fines content), which would affect the lateral spreading displacements. However, it is very likely, that these corestones are not playing a key role in the liquefaction susceptibility of the material and the characteristics of the soil matrix are controlling the behavior. In that context, the estimates by the [85] equation should be considered approximate performance indicators at best.

7.1. Lixouri Port area

Considering the variation of the quay wall height, H, and the locations of the eight transects surveyed in the Lixouri Port, the transects were divided into three groups each having a similar average height, i.e. $H_{avg} = 7.6$ m (TS-3, TS-4, four stack blocks), $H_{avg} = 4.4$ m (TS-1, TS-2, TS-5, TS-6, two stack blocks), and $H_{avg} = 2.6$ m (TS-7, TS-8, single stack blocks). The three plots of Fig. 22 depict the distribution of measured cumulative horizontal ground displacements, D_H (including mean and ±1SD curves) with distance, L, as well as the distribution of

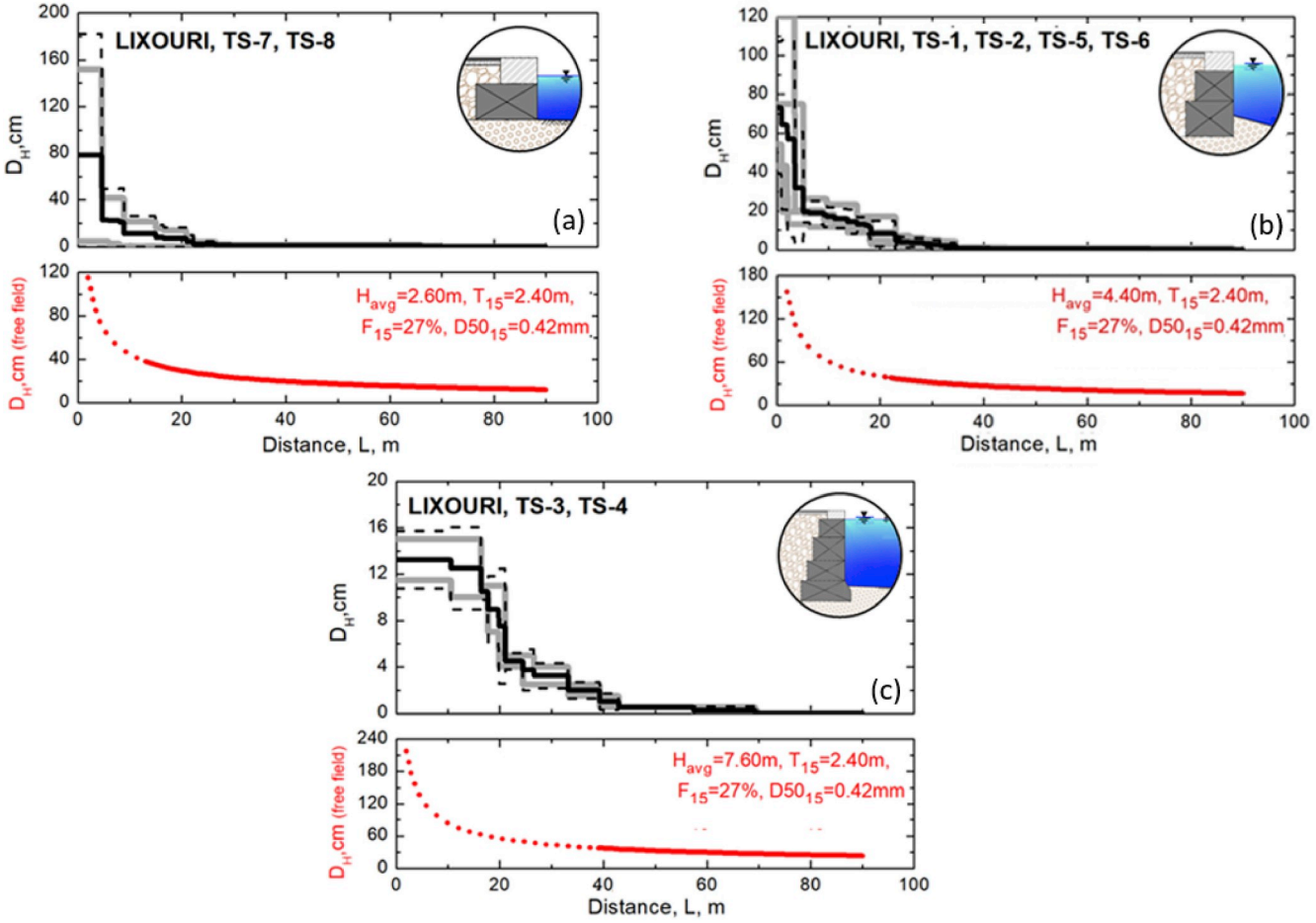

Fig. 22. Distribution of measured cumulative lateral spreading displacements for three groups of transects in the Lixouri Port area vs. predicted values from the [85] model shown with red color (dotted line segment indicates lower reliability in prediction as suggested by Ref. [85]. (For interpretation of the references to color in this figure legend, the reader is referred to the Web version of this article.)

corresponding values predicted by the [85] equation.

The plots of Fig. 22(a) indicate that at the south section of the Lixouri port front (TS-7 & TS-8) - where the single block quay walls have a small height (≤2.6 m) - the measured lateral displacements are in relatively good agreement with the corresponding free field values (estimated from the [85] equation). More specifically, it is observed that the assumption of free field conditions results in an overprediction of lateral spreading in the vicinity of the quay wall that is less than 100%. As the height and weight of the quay wall is increased, however, the assumption of free field conditions leads to a considerable overprediction of lateral spreading: approximately three times higher than the average of measured lateral displacements for H = 4.4 m (Fig. 22(b)) and about an order of magnitude higher for the case of high (H = 7.6 m) quay walls at the north section of the port, Fig. 22(c). It is also important to note that the length behind the port front of the affected area by lateral displacements is significantly shorter than predicted for the free field conditions.

It may thus be concluded that the lateral ground displacements likely to occur in the land area of ports with high quay walls are significantly lower than the values predicted by the available empirical methods assuming free field (and in particular free face) conditions. It should be noted that the predicted magnitudes of lateral spreading for free field conditions indicate a very high to high damage potential in the affected area (according to Ref. [54] classification), which is consistent with the observed damage.

7.2. Argostoli Port area

The plots of Fig. 23 illustrate comparisons between measured cumulative horizontal ground displacements and corresponding predictions based on the free-field assumption, for four groups of transects located behind progressively higher quay walls (H = 0.8 m to H = 6.5 m) at the Argostoli Port area. It may be again observed that for the cases of small quay walls (H ≤ 2.5 m) the free field values are consistent with the field observations (i.e., they over- or under-predict the expected lateral movements by approximately 100%). On the other hand, for higher quay walls (H = 3 m to H = 6.5 m) the overprediction of lateral displacements using free-field conditions reaches (or exceeds) an order of magnitude. It is also observed that the measured inland extent of the lateral displacements is always shorter than predicted by the free-field empirical equation.

It is also worth noting that the empirically predicted values of free-field lateral spreading magnitudes indicate low to moderate damage potential [54], consistent with the observed behavior.

The results of measurements at the ports of Lixouri and Argostoli indicate that empirical predictions of lateral spreading magnitudes should not be used in the case of land areas of ports with high and heavy quay walls.

8. Summary and conclusions

The 2014 Cephalonia, Greece (M_w 6.1 & 6) earthquake doublet caused soil liquefaction, mainly in the port areas of Lixouri and

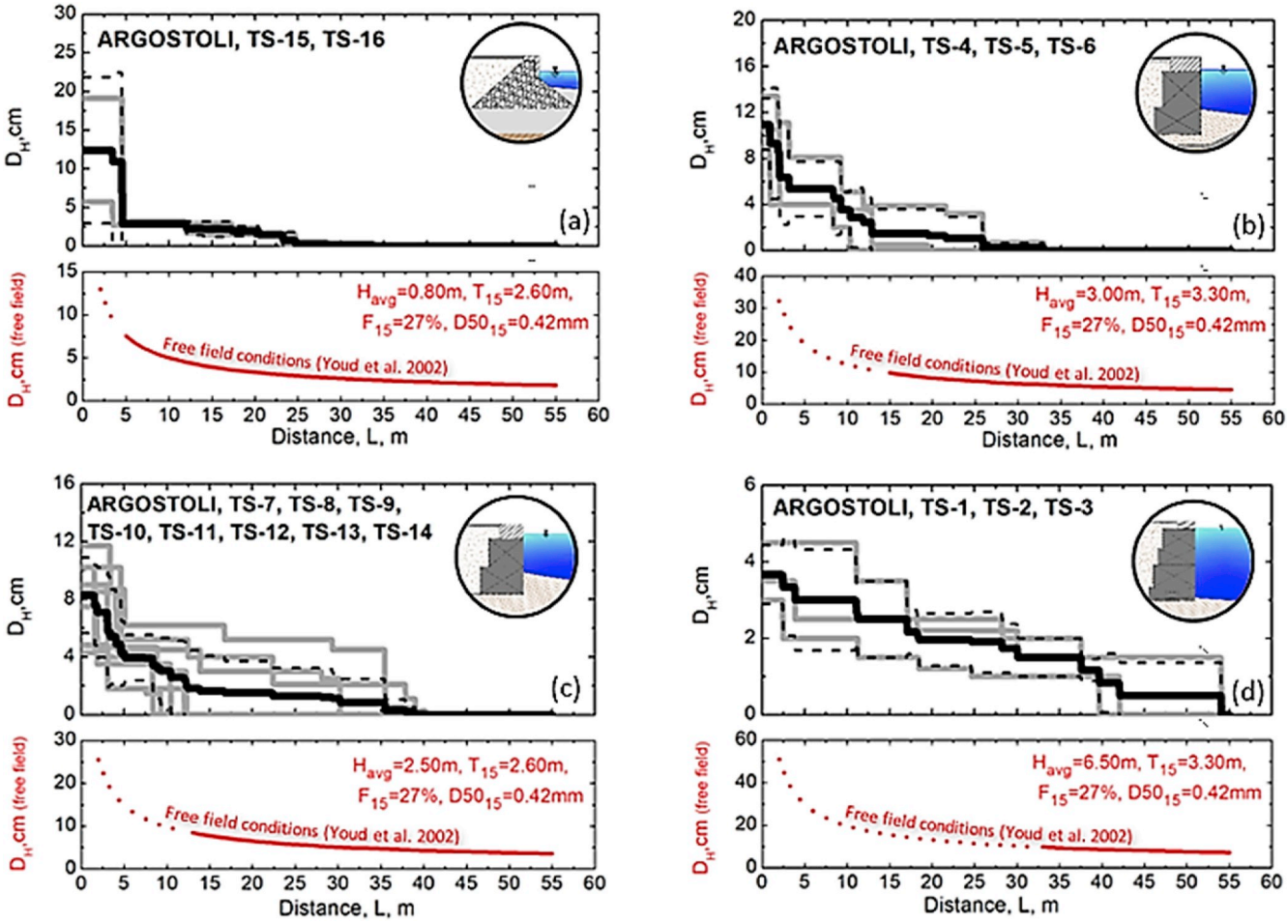

Fig. 23. Distribution of measured cumulative lateral spreading displacements for three groups of transects in the Argostoli port area vs. predicted values from the [85] model shown with red color (dotted line segment indicates lower reliability in prediction as suggested by Ref. [85]. (For interpretation of the references to color in this figure legend, the reader is referred to the Web version of this article.)

Argostoli, which was manifested by sandy and gravelly boils and lateral spreading of the ground towards the free face of the quay walls of the two ports. The results of lateral ground displacement measurements, performed by ground surveys, in the areas of Port of Lixouri and Port of Argostoli were presented along with seismotectonic, strong motion and available geotechnical data. The results of field measurements using interpreted geometric, seismic and soil parameters were compared to the empirical predictions of the [85] relationship, which was developed for free field conditions to assess the effects of the quay walls in reducing the magnitude of lateral spreading. The following conclusions can be drawn:

1. The magnitude of liquefaction-induced lateral spreading in the Lixouri Port area ranged from 4 cm to 152 cm. It is noted, however, that some of the high values of measured horizontal ground displacements may have included the seaward horizontal displacement of the quay walls of the port which according to geodetic measurements were found to range between 0.27 m and 0.45 m in the main pier of Lixouri Port. The high values of ground displacements in Lixouri may also have been influenced by forward directivity effects. The measured lateral displacements of the Argostoli Port area were smaller - by about an order of magnitude - and ranged from 3 cm to 20 cm. The inland maximum lateral extent of horizontal ground movement at the two port areas (Lixouri and Argostoli) was found to be 95 m and 55 m, respectively.
2. The subsurface conditions at the land areas of Lixouri and Argostoli Ports are generally similar: reclamation fills of varying thickness overlying fine-grained deposits. The thickness of the liquefied layer, T_{15}, in the Lixouri Port was estimated to be equal to 2.4 m, whereas in the Argostoli Port area it ranged from 2.6 m to 3.3 m. These values of T_{15} - which are admittedly characterized by some degree of uncertainty – were used to estimate the predicted lateral spreading displacements for free-field conditions.
3. The magnitude of lateral spreading that occurs as a result of earthquake shaking in the land area of ports with gravity type (multi-block) quay walls, is significantly reduced, compared to the values predicted for free-field conditions for large quay walls. The over-prediction resulting from the use of existing empirical relations may be as much as an order of magnitude for the case of high gravity type quay walls. On the other hand, for small retaining structures the predicted displacements were comparable to the measured displacements (i.e., under- or over-prediction was less than 100%).
4. The observed seismic damage to the marine structures of the Lixouri Port and the lack of similar damage at the Argostoli Port are consistent with published damage potential criteria based on the magnitude of liquefaction-induced free field lateral spreading displacements.

Acknowledgments

The field performance data collected was part of a broader Geotechnical Engineering Extreme Events reconnaissance expedition (GEER). This expedition was partially funded through a National Science Foundation (NSF) Grant No. CMMI-1266418 through GEER

(http://geerassociation.org/) and the Laboratory of Geotechnical Engineering, Dept. of Civil Engineering, University of Patras. Additional partial funding was provided by the National Science Foundation (NSF) Grant No. CMMI- 1663288. Any opinions, findings, and conclusions or recommendations expressed in this material are those of the authors and do not necessarily reflect the views of the NSF.

APPENDIX

Geometries of quay walls in Lixouri port in locations shown in Fig. 22 and Fig. 23.

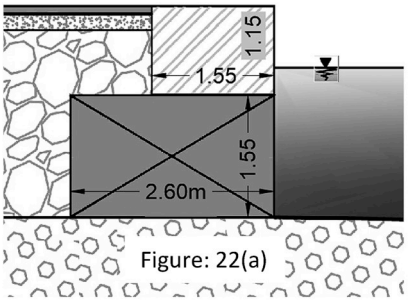

Figure: 22(a)

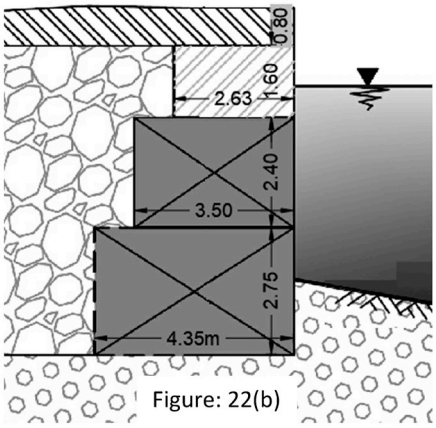

Figure: 22(b)

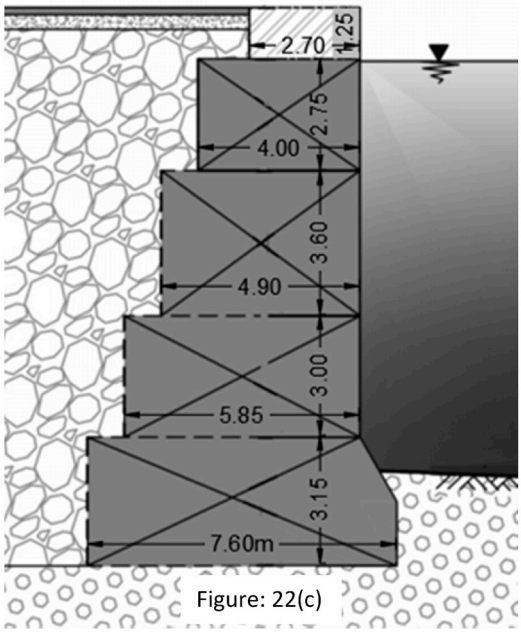

Figure: 22(c)

Geometries of quay walls in Argostoli port in locations shown in Fig. 23.

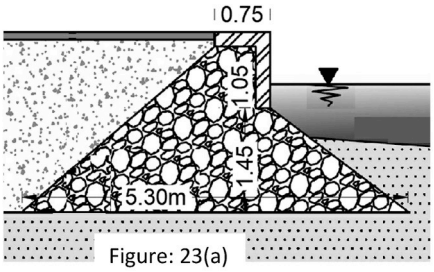

Figure: 23(a)

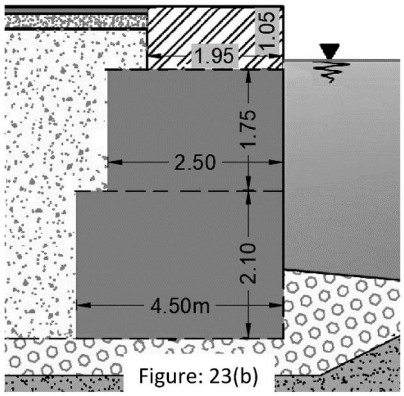

Figure: 23(b)

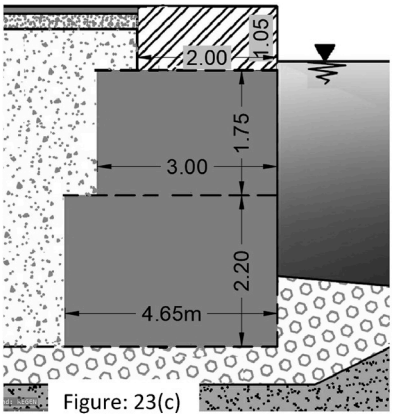

Figure: 23(c)

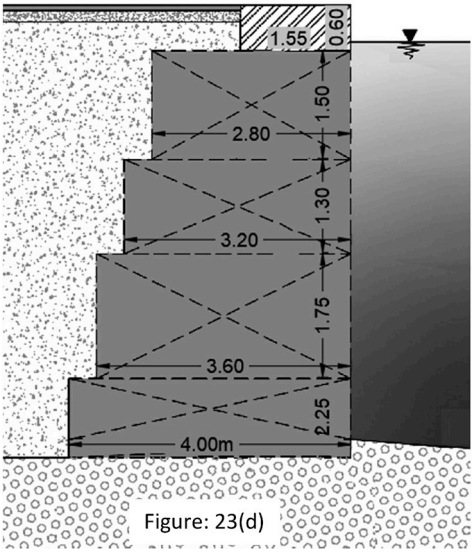

Figure: 23(d)

References

[1] Abdoun T, Oskay C, Wang Y, Zeghal M. Visualization of measured quay wall seismic response. In: Proc. of the 15th ICSMGE, Istanbul, 2. A.A.BALKEMA; 2001. p. 1057–60.

[2] Ambraseys N. Earthquakes in the Mediterranean and Middle East: a multidisciplinary study of seismicity up to 1900. Cambridge University Press; 2009.

[3] Applegate KN. Evaluation of liquefaction-induced lateral spreading in the Midwest, M.S. in Civil Engineering. Missouri University of Science and Technology; 2010.

[4] Athanasopoulos G,A. Empirical correlations vs-NSPT for soils of Greece: a comparative study of reliability. In: Cakmak A,S, editor. Proceedings of 7th international conference on soil dynamics and earthquake engineering, chania, crete. Southampton: Computational Mechanics; 1995. p. 19–36.

[5] Athanasopoulos-Zekkos A. Personal communication; data provided for authors use. 2018. but not publication.

[6] Bartlett SF, Youd TL. Empirical prediction of liquefaction-induced lateral spread. J. Geotech. Eng. 1995;121–4:316–29.

[7] Bastin S, Cubrinovski M, van Ballegooy S, Russell J. Geologic and geomorphic influences on the spatial extent of lateral spreading in Christchurch, New Zealand. In: 3rd international Conference on performance-based design in earthquake geotechnical Engineering (PBDIII), Vancouver; 2017.

[8] Batilas A, Pelekis P, Vlachakis V, Athanasopoulos G. Soil liquefaction/nonliquefaction in the Achaia-Ilia (Greece) 2008 earthquake: field evidence, site characterization and ground motion Assessment. ISSMGE International Journal of Geoengineering Case Histories 2014;2(4):270–87.

[9] Batilas AV, Pelekis PC, Roussos PG, Athanasopoulos GA. SPT energy measurements: manual vs. Automatic hammer release. Geotech Geol Eng 2016;35(2):879–88.

[10] Baziar MH, Saeedi Azizkandi A. Evaluation of lateral spreading utilizing artificial neural network and genetic programming. Int J Civ Eng 2013;(2):100–11.

[11] Benekos G, Derdelakos K, Bountzouklis C, Kourkouli P, Parcharidis I. Surface displacements of the 2014 Cephalonia (Greece) earthquake using high resolution SAR interferometry. Earth Sci India 2015;8(2):309–15.

[12] Boissier E. The february 2014 Cephalonia earthquake (Greece): 3D deformation field and source modeling from multiple SAR techniques. https://discuss.terradue.com/t/the-february-2014-cephalonia-earthquake-greece-3d-deformation-field-and-source-modeling-from-multiple-sar-techniques/34; 2015.

[13] Boulanger RW, Idriss IM. CPT and SPT based liquefaction triggering procedures. Report No. UCD/CGM.-14. 2014. p. 1.

[14] Boulanger RW, Idriss IM. Liquefaction susceptibility criteria for silts and clays. J. of Geotechnical and Geoenvironmental Engineering, ASCE 2006;132(No. 11):1413–26.

[15] Bowen HJ, Jacka ME, Van Ballegooy S, Sinclair TJE, Cowan H. "Lateral spreading in the Canterbury earthquakes–Observations and empirical prediction methods". In: Proceedings of 15th world conference on earthquake engineering; 2012.

[16] Bray JD, Sancio RB. Assessment of the liquefaction susceptibility of fine-grained soils. ASCE. Journal of Geotechnical and Geoenvironmental Engineering 2006;132(9):1165–77.

[17] Bray JD, Boulanger RW, Cubrinovski M, Tokimatsu K, Kramer SL, O'Rourke T, et al. U.S.–New Zealand–Japan international Workshop, liquefaction-induced ground movement effects. PEER Report 2017/02. Pacific Earthquake Engineering Research Center; 2017.

[18] Bray J, Rollins K, Hutchinson T, Verdugo R, Ledezma C, Mylonakis G, et al. Effects of ground failure on buildings, ports, and industrial facilities. Earthq Spectra 2012; 28(S1):S97–118.

[19] Briole P, Elias P, Parcharidis I, Bignami C, Benekos G, Samsonov S, Kyriakopoulos C, Stramondo S, Chamot-Rooke N, Drakatou ML, Drakatos G. The seismic sequence of January–February 2014 at Cephalonia Island (Greece): constraints from SAR interferometry and GPS. Geophysical Supplements to the Monthly Notices of the Royal Astronomical Society 2015;203(3):1528–40.

[20] Cetin KO, Youd TL, Seed RB, Bray JD, Stewart JP, Durgunoğlu HT, et al. Liquefaction-induced lateral spreading at Izmit bay during the Kocaeli (Izmit)-Turkey earthquake. ASCE. Journal of Geotechnical and Geoenvironmental Engineering 2004;130(12):1300–13.

[21] Chu DB, Stewart JP, Youd TL, Chu BL. Liquefaction-induced lateral spreading in near-fault regions during the 1999 Chi-Chi, Taiwan earthquake. ASCE. Journal of Geotechnical and Geoenvironmental Engineering 2006;132(12):1549–65.

[22] Cubrinovski M, Robinson K, Taylor M, Hughes M, Orense R. Lateral spreading and its impacts in urban areas in the 2010–2011 Christchurch earthquakes. N Z J Geol Geophys 2012;55(3):255–69.

[23] Cubrinovski M, Winkley A, Haskell J, Palermo A, Wotherspoon L, Robinson K, Hughes M. Spreading-induced damage to short-span bridges in Christchurch, New Zealand. Earthq Spectra 2014;30(1):57–83.

[24] Dobry R, Abdoun T. Recent studies on seismic centrifuge modeling of liquefaction and its effect on deep foundations. In: 4th international conference on recent advances in geotechnical earthquake engineering and soil dynamics; 2001. p. 30.

[25] Dobry R, Thevanayagam S, Medina C, Bethapudi R, Elgamal A, Bennett V, et al. Mechanics of lateral spreading observed in a full-scale shake test. ASCE. Journal of Geotechnical and Geoenvironmental Engineering 2011;137(2):115–29.

[26] Ekstrom LT, Franke KW. Simplified procedure for the performance-based prediction of lateral spread displacements. J Geotech Geoenviron Eng 2016;142(7): 04016028.

[27] Elgamal A, Yang Z. Numerical modeling of liquefaction-induced lateral spreading. In: Proceedings of 12 WCEE; 2000.

[28] Elgamal A, Lu J, Forcellini D. Mitigation of liquefaction-induced lateral deformation in a sloping stratum: three-dimensional numerical simulation. J Geotech Geoenviron Eng 2009;135(11):1672–82.

[29] Fiegel GL, Kutter BL. "Liquefaction mechanism for layered soils". ASCE. Journal of Geotechnical Engineering 1994;120(12):2236–43.

[30] Franke KW, Kramer SL. Procedure for the empirical evaluation of lateral spread displacement hazard curves. ASCE 2014.

[31] Ganas A, Cannavo F, Chousianitis K, Kassaras I, Drakatos G. Displacements recorded on continuous GPS stations following the 2014 M6 Cephalonia (Greece) earthquakes: dynamic characteristics and kinematic implications. Acta Geodyn Geomater 2015;12(1):177.

[32] Garini E, Gazetas G. Rocking and sliding potential of the 2014 Cephalonia, Greece earthquakes. In: ICONHIC2016 1st international conference on natural hazards & infrastructure June, Chania, Greece; 2016.

[33] Garini E, Gazetas G, Anastasopoulos I. Evidence of significant forward rupture directivity aggravated by soil response in an M_w6 earthquake and the effects on monuments. Earthq Eng Struct Dyn 2017;46(13):2103–20.

[34] Gazetas G, Garini E. The 2014 Cephalonia twin earthquakes: the seismic failure of memorial columns verify the strong directivity effect. In: 3rd international conference on performance-based design in earthquake geotechnical engineering, PBDIII, Vancouver, BC, Canada; 2017.

[35] GEER/EERI/ATC. Earthquake reconnaissance January 26th/February 2nd 2014 Cephalonia, Greece events. Version 1: June 6. 2014.

[36] Ghasemi-Fare O, Pak A. Prediction of lateral spreading displacement on gently sloping liquefiable ground. In: Geotechnical Frontiers, ASCE GSP 281; 2017. p. 267–76.

[37] Gillins DT, Bartlett S. Multilinear regression equations for predicting lateral spread displacement from soil type and Cone penetration test data. In: American Society of Civil Engineers. © ASCE 04013047-1 J. Geotech. Geoenviron. Eng; 2013.

[38] Hamada, Towhata I, Yasuda S, Isoyama R. Study on permanent ground displacement induced by seismic liquefaction. Comput. Geotech 1986;4:197–220. Elsevier Applied Science Publication.

[39] Hubler J, Athanasopoulos-Zekkos A, Zekkos D. Monotonic and cyclic simple shear response of gravel-sand mixtures. Soil Dyn Earthq Eng 2018;115:291–304.

[40] Hubler J, Athanasopoulos-Zekkos A, Zekkos D. Monotonic, cyclic and post-cyclic simple shear response of three Uniform gravels in constant volume conditions. ASCE Journal of Geotechnical and Geoenvironmental Engineering 2017;143(9). https://doi.org/10.1061/(ASCE)GT.1943-5606.0001723.

[41] Ishihara K, Yoshida K, Kato M. Characteristics of lateral spreading in liquefied deposits during the 1995 Hanshin-Awaji earthquake. J Earthq Eng 1997;1(1): 23–55.

[42] Kalantary F, MolaAbasi H, Salahi M, Veiskarami M. Prediction of liquefaction induced lateral displacements using robust optimization model. Sci Iran 2013;20 (2):242–50.

[43] Kamai R, Boulanger RW. Simulations of a centrifuge test with lateral spreading and void redistribution effects. J Geotech Geoenviron Eng 2013;139(8):1250–61.

[44] Karakostas V, Papadimitriou E, Mesimeri M, Gkarlaouni C, Paradisopoulou P. The 2014 Kefalonia doublet (M_w 6.1 and M_w 6.0), central Ionian islands, Greece: seismotectonic implications along the Kefalonia transform fault zone. Acta Geophys 2015;63(1):1–16.

[45] Karastathis VK, Mouzakiotis E, Ganas A, Papadopoulos GA. High-precision relocation of seismic sequences above a dipping Moho: the case of the January-February 2014 seismic sequence on Cephalonia island (Greece). Solid Earth 2015;6 (1):173–84.

[46] Karastathis VK, Mouzakiotis E, Ganas A, Papadopoulos GA. High-precision relocation of seismic sequences above a dipping Moho: the case of the January-February 2014 seismic sequence in Cephalonia island (Greece). Solid Earth Discussions 2014;6:2699–733.

[47] Kavazanjian Jr E, 11 more authors. State of the art and practice in the assessment of earthquake-induced soil liquefaction and its Consequences. Washington, DC: The National Academies Press; 2016. https://doi.org/10.17226/23474.

[48] Kokusho T. Water film in liquefied sand and its effect on lateral spread. ASCE. Journal of Geotechnical and Geoenvironmental Engineering 1999;125(10): 817–26.

[49] Kramer S,L, Makdisi A,J. Applicability of sliding block analyses to lateral spreading problems. In: 3rd international conference on performance-based design in earthquake geotechnical engineering (PBDIII), Vancouver; 2017.

[50] Kutter BL, Gajan S, Manda KK, Balakrishnan A. Effects of layer thickness and density on settlement and lateral spreading. J Geotech Geoenviron Eng 2004;130 (6):603–14.

[51] Lekkas EL, Mavroulis SD. Fault zones ruptured during the early 2014 Cephalonia Island (Ionian Sea, Western Greece) earthquakes (January 26 and February 3, Mw 6.0) based on the associated co-seismic surface ruptures. J Seismol 2016;20(1): 63–78.

[52] Mavroulis S, Carydis P, Alexoudi V, Grambas A, Lekkas E. The January–february 2014 Cephalonia (Ionian Sea, western Greece) earthquakes: tectonic and seismological aspects. In: Proceedings of the 16th world conference on earthquake engineering (16WCEE), Paper No 413; 2017.

[53] Merryman Boncori JP, Papoutsis I, Pezzo G, Tolomei C, Atzori S, Ganas A, Karastathis V, Salvi S, Kontoes C, Antonioli A. The February 2014 Cephalonia earthquake (Greece): 3D deformation field and source modeling from multiple SAR techniques. Seismol Res Lett 2015;86(1):124–37.

[54] Moriarty M,D. Evaluation of damage induced by lateral spread to roadways and bridges in Salt Lake County. MSc Thesis. Dept. of Civil and Environmental Engineering, University of Utah; 2014. p. 147.

[55] Munter SK, Boulanger RW, Krage CP, DeJong JT. Evaluation of liquefaction-induced lateral spreading procedures for interbedded deposits: Çark canal in the 1999 M7.5 Kocaeli earthquake. ASCE GSP281, Geotechnical Frontiers 2017 2017: 254–66.

[56] Nikolaou S, Ramon Gilsanz PE, SE F, Iliadelis D, Pehlivan M, Mahvashmohammadi A, et al. Learning from structural success rather than failures. Structure 2015;26.

[57] Nikolaou S, Zekkos D, Asimaki D, Gilsanz R. Reconnaissance highlights of the 2014 sequence of earthquakes in Cephalonia, Greece. In: 6th int. Conf. on earthquake geotechnical engineering, christchurch. London: International Society for Soil Mechanics and Geotechnical Engineering, ISSMGE; 2015.

[58] Olson SM, Johnson CI. Analyzing liquefaction-induced lateral spreads using strength ratios. J Geotech Geoenviron Eng 2008;134(8):1035–49.

[59] Papadopoulos GA, Karastathis VK, Koukouvelas I, Sachpazi M, Baskoutas I, Chouliaras G, Mouzakiotis A. The Cephalonia, Ionian Sea (Greece), sequence of strong earthquakes of January-February 2014: a first report. Res Geophys 2014;4 (1).

[60] Papathanasiou G, Ganas A, Valkaniotis S, Papanikolaou M, Pavlides S. Preliminary report on the geological effects triggered by the 2014 Cephalonia earthquakes. AUTH: National Observatory of Athens, Institute of Geodynamics – School of Geology; 2014.

[61] Papathanassiou G, Ganas A, Valkaniotis S. Recurrent liquefaction-induced failures triggered by 2014 Cephalonia, Greece earthquakes: spatial distribution and quantitative analysis of liquefaction potential. Eng Geol 2016;200:18–30.

[62] Papazachos B, Papazachou C. The earthquakes of Greece. third ed. Thessaloniki: Ziti Public; 2003. p. 286.

[63] PIANC. "Seismic design guidelines for port structures", report of Working group No 34 of the Maritime navigation Commission. International Navigation Association; 2001. p. 43p.

[64] Rathje EM, Secara SS, Martin JG, van Ballegooy S, Russell J. Liquefaction-induced horizontal displacements from the Canterbury earthquake sequence in New Zealand measured from remote sensing techniques. Earthq Spectra 2017;33(4): 1475–94.

[65] Rauch AF, James RM. EPOLLS model for predicting average displacements on lateral spreads. J Geotech Geoenviron Eng 2000.

[66] Robinson K, Cubrinovski M, Bradley BA. Lateral spreading displacements from the 2010 Darfield and 2011 Christchurch earthquakes. Int J Geotech Eng 2014;8(4): 441–8.

[67] Robinson K, Cubrinovski M, Kailey P, Orense R. Field measurements of lateral spreading following the 2010 Darfield earthquake. In: Proceedings of the Ninth pacific conference on earthquake engineering; 2011. p. 52–9.

[68] Russell, J., van Ballegooy, S., Bastin, S., Cubrinovski, M., Ogden, M. "Influence of geometric, geologic, geomorphic and subsurface ground conditions on the accuracy of empirical models for prediction of lateral spreading." Proceedings of PBD - III, [Vancouver, Canada].

[69] Sakkas V, Lagios E. Ground deformation effects from the~ M6 earthquakes (2014–2015) on Cephalonia–Ithaca Islands (Western Greece) deduced by GPS observations. Acta Geophys 2017;65(1):207–22.

[70] Sakkas V, Lagios E. Fault modelling of the early-2014~ M6 Earthquakes in Cephalonia Island (W. Greece) based on GPS measurements. Tectonophysics 2015; 644:184–96.

[71] Sato M, Mohajeri M, Abe A. Large scale shake table test on lateral spreading of liquefied sand behind a sheet pile wall model. In: Proceedings of 13th world conference on earthquake engineering; 2004. p. 1–6.
[72] Shamoto Y, Zhang J, Tokimatsu K. New charts for predicting large residual post-liquefaction ground deformations. Soil Dyn Earthq Eng, 17. New York: Elsevier; 1998. p. 427–38.
[73] Shooshpasha I, MolaAbasi H. Prediction of liquefaction induced lateral displacements using plynomial neural networks and genetic Algorithms. In: 15th world conference on earthquake engineering, Lisbon, Portugal; 2012, September.
[74] Sokos E, Kiratzi A, Gallovič F, Zahradník J, Serpetsidaki A, Plicka V, Jansky J, Kostelecky J, Tselentis GA. Rupture process of the 2014 Cephalonia, Greece, earthquake doublet (Mw6) as inferred from regional and local seismic data. Tectonophysics 2015;656:131–41.
[75] Stiros SC, Pirazzoli PA, Laborel J, Laborel-Deguen F. The 1953 earthquake in Cephalonia (Western Hellenic Arc): coastal uplift and halotectonic faulting. Geophys J Int 1994;117(3):834–49.
[76] Sugano T, Kohama E. Seismic performance of Urban, reclaimed, and port areas-full scale experiment using Blast technique. In: Cauffman Stephen A, editor. NIST special publication 987, Proceedings of the 14th Joint panel Meeting; 2002.
[77] Taboada-Urtuzuastegui VM, Dobry R. Centrifuge modeling of earthquake-induced lateral spreading in sand. ASCE. Journal of Geotechnical and Geoenvironmental Engineering 1998;124(12):1195–206.
[78] Theodoulidis N, Karakostas C, Lekidis V, Makra K, Margaris B, Morfidis K, Savvaidis A. The Cephalonia (Greece) earthquakes of January 26 and February 3, 2014: effects on soil and built environment. In: 2nd europ. Conf. on earthquake engineering and seismology (2ECEES), 25-29 August 2014, Istanbul, Turkey; 2014.
[79] Theodoulidis N, Karakostas C, Lekidis V, Makra K, Margaris B, Morfidis K, Papaioannou C, Rovithis E, Salonikios T, Savvaidis A. The Cephalonia, Greece, January 26 (M6. 1) and February 3, 2014 (M6. 0) earthquakes: near-fault ground motion and effects on soil and structures. Bull Earthq Eng 2015;14(1):1–38.
[80] Tryon GE. Evaluation of Current empirical methods for predicting lateral spread-induced ground deformations for large magnitude earthquakes using Maule Chile 2010 Case histories. Msc thesis. Brigham Young University; 2014.
[81] Valkaniotis S, Ganas A, Papathanassiou G, Papanikolaou M. "Field observations of geological effects triggered by the January–february 2014 Cephalonia (Ionian Sea, Greece) earthquakes". Tectonophysics 2014;630:150–7.
[82] Valsamis A, Bouckovalas G, Dimitriadi V. Parametric investigation of lateral spreading in free-face ground formations. 2010.
[83] Valsamis A, Bouckovalas G, Dimitriadi V. Numerical evaluation of lateral spreading displacements in layered soils. In: Proceedings of the 4th international conference on earthquake geotechnical engineering (4ICEGE), Thessaloniki, Greece, June; 2007, June. p. 25–8.
[84] Youd TL. Application of MLR procedure for prediction of liquefaction-induced lateral spread displacement. ASCE, Journal of Geotechnical and Geoenvironmental Engineering 2018;144(6):04018033.
[85] Youd TL, Hansen CM, Bartlett SF. Revised multilinear regression equations for prediction of lateral spread displacement. Journal of Geotechnical and Geoenvironmental Engineering, ASCE, December 2002;2002:1007–17.
[86] Zekkos D, Manousakis J, Greenwood W, Lynch J. June). Immediate UAV-enabled infrastructure reconnaissance following recent natural disasters: case histories from Greece. In: International conference on natural hazards and infrastructure; 2016.
[87] Zekkos D, Greenwood W, Manousakis J, Athanasopoulos-Zekkos A, Clark M, Cook KL, Saroglou C. Lessons learned from the Application of UAV-enabled structure-from-motion photogrammetry in geotechnical engineering. International Journal of Geoengineering Case Histories 2018;4(4):254–74. https://doi.org/10.4417/IJGCH-04-04-03.
[88] Zhang G, Robertson PK, Brachman RWI. Estimating liquefaction-induced lateral displacements using the standard penetration test or cone penetration test. J Geotech Geoenviron Eng 2004;130(8):861–71.
[89] Zhang J, Zhao JX. Empirical models for estimating liquefaction-induced lateral spread displacement. Soil Dyn Earthq Eng 2005;25(6):439–50.
[90] Zhang J, Beetham D, Dellow G, Zhao JX, McVerry GH. Empirical models for predicting lateral spreading and evaluation using New Zealand data. Bull N Z Soc Earthq Eng 2008;41(1):10Á23.